

LES validation of urban flow, part I: flow statistics and frequency distributions

Article

Accepted Version

Hertwig, D. ORCID: <https://orcid.org/0000-0002-2483-2675>, Patnaik, G. and Leidl, B. (2017) LES validation of urban flow, part I: flow statistics and frequency distributions. *Environmental Fluid Mechanics*, 17 (3). pp. 521-550. ISSN 1567-7419 doi: <https://doi.org/10.1007/s10652-016-9507-7> Available at <https://centaur.reading.ac.uk/76907/>

It is advisable to refer to the publisher's version if you intend to cite from the work. See [Guidance on citing](#).

To link to this article DOI: <http://dx.doi.org/10.1007/s10652-016-9507-7>

Publisher: Springer

All outputs in CentAUR are protected by Intellectual Property Rights law, including copyright law. Copyright and IPR is retained by the creators or other copyright holders. Terms and conditions for use of this material are defined in the [End User Agreement](#).

www.reading.ac.uk/centaur

CentAUR

Central Archive at the University of Reading

Reading's research outputs online



1 **LES validation of urban flow, part I: flow statistics and**
2 **frequency distributions**

3 **Denise Hertwig · Gopal Patnaik · Bernd Leitl**

4
5 Received: date / Accepted: date

6 **Abstract** Essential prerequisites for a thorough model evaluation are the availability of
7 problem-specific, quality-controlled reference data and the use of model-specific compar-
8 ison methods. The work presented here is motivated by the striking lack of proportion be-
9 tween the increasing use of large-eddy simulation (LES) as a standard technique in micro-
10 meteorology and wind engineering and the level of scrutiny that is commonly applied to as-
11 sess the quality of results obtained. We propose and apply an in-depth, multi-level validation
12 concept that is specifically targeted at the time-dependency of mechanically induced shear-
13 layer turbulence. Near-surface isothermal turbulent flow in a densely built-up city serves
14 as the test scenario for the approach. High-resolution LES data are evaluated based on a
15 comprehensive database of boundary-layer wind-tunnel measurements.

16 From an exploratory data analysis of mean flow and turbulence statistics, a high level
17 of agreement between simulation and experiment is apparent. Inspecting frequency distri-
18 butions of the underlying instantaneous data proves to be necessary for a more rigorous
19 assessment of the overall prediction quality. From velocity histograms local accuracy limi-

D. Hertwig
Meteorological Institute, University of Hamburg
Bundesstrasse 55, D-20146 Hamburg, Germany
Present address:
Department of Meteorology, University of Reading
P.O. Box 243, Reading, RG6 6BB, UK
E-mail: d.hertwig@reading.ac.uk
Tel.: +44-118-378-6721
Fax: +44-118-378-8905

G. Patnaik
Laboratories for Computational Physics and Fluid Dynamics
U.S. Naval Research Laboratory
Washington D.C., USA
E-mail: gopal.patnaik@nrl.navy.mil

B. Leitl
Meteorological Institute, University of Hamburg
Bundesstrasse 55, D-20146 Hamburg, Germany
E-mail: bernd.leitl@uni-hamburg.de

tations due to a comparatively coarse building representation as well as particular strengths of the model to capture complex urban flow features with sufficient accuracy are readily determined. However, the analysis shows that further crucial information about the physical validity of the LES needs to be obtained through the comparison of eddy statistics, which is focused on in part II.

Compared with methods that rely on single figures of merit, the multi-level validation strategy presented here supports conclusions about the simulation quality and the model's fitness for its intended range of application through a deeper understanding of the unsteady structure of the flow.

Keywords Large-eddy simulation · Model validation · Quality assurance · Turbulent flow · Urban environment · Wind tunnel

1 Introduction

Unsteady flow in built environments is an important representative of the complex nature of near-surface atmospheric turbulence. Studying and characterising urban flow fields is of strong practical interest with regard to issues like urban ventilation and pollutant dispersion, wind and thermal comfort, heat and moisture transfer and other urban micro-climatic processes [17,32,60,42,43]. Such problems cannot easily be investigated by means of classic *in-situ* measurements, making high-resolution computational fluid dynamics (CFD) simulations increasingly attractive for wind engineering and micro-meteorological communities [45,34,61,62].

Obstacle-resolving micro-scale meteorological models based on the Reynolds-averaged Navier-Stokes (RANS) equations are routinely applied to investigate urban flow and dispersion phenomena, e.g. [27,65]. Rapid advancements in computer capacities over the last 15 years or so, however, have increased the use of turbulence-resolving numerical approaches like large-eddy simulation (LES) for similar applications on the urban scale [61]. In contrast to RANS simulations, eddy-resolving approaches have the potential to adequately reproduce complex turbulent flow regimes together with their temporal evolution [30].

Comparative studies have revealed advantages of urban LES over steady-state RANS approaches on the mean-flow level. Xie and Castro [72] for example compared LES and RANS predictions of flow over a cube array to wind-tunnel measurements and data from direct numerical simulation. While the accuracy of RANS was found to be comparable to LES well above the urban canopy layer (UCL), it deteriorates below rooftop. The better performance of LES in the UCL was attributed to the ability to capture unsteady urban flow features. Similar conclusions were drawn by Salim et al. [54] for pollutant dispersion in a street canyon and by Tominaga and Stathopoulos [63,64], who compared RANS and LES dispersion fields within an isolated street and a cube array. In both configurations, the LES results were in better agreement with the reference experiments and provided a more realistic picture of the characteristics of the pollutant plume.

Most of today's published studies on urban LES were conducted in strongly idealised urban environments (e.g. isolated buildings, isolated street canyons, idealised building arrays). However, in recent years the complexity of the flow problems being analysed has increased. LES studies of flow and dispersion in realistic urban settings and in larger domains, extending into neighbourhood and city scales are now available as well [51,73,41]. Other studies have focused on advancing the level of physical complexity covered by the simulations, e.g. by representing atmospheric stability effects [74], differential heating of urban surfaces [19, 49,38,39] or aerodynamic effects of urban greenery [44].

66 The focus of the work presented here is put on how the quality of such turbulence-
67 resolving simulations can be assessed and quantified by taking into account the time-depen-
68 dent nature of the model output.

69 A thorough validation of the model is a crucial step in establishing confidence in its
70 skill and reliability and to assess possible bounds of uncertainty for cases in which the truth
71 is not known *a priori*. The first important step for validating numerical models is finding
72 reliable, reproducible reference data that provide detailed information about important flow
73 parameters, against which the model performance and uncertainty can be assessed. Due to
74 the increase of information about unsteady flow dynamics available from LES there is an
75 increasing demand on the overall quantity of reference data and the level of detail about the
76 flow that can be derived from such data [2,35]. In order to avoid incorrectly accepting the
77 time-resolved model results as the “ground truth” [71], strategies pursued in LES validation
78 have to provide information of whether the simulation adequately reproduces the spatial-
79 temporal behaviour of turbulent eddies in the flow. While validation standards for RANS-
80 type simulations have been defined in the past [67, 15, 16, 55], as of now there has been no
81 similar community-wide effort leading to similar consensus about standards for an in-depth
82 validation of LES.

83 Since the non-linear nature of turbulence precludes the direct comparison of instanta-
84 neous fields or time series from experiment and LES, the validation has to rely on statisti-
85 cal approaches. As commonly done with RANS results, comparisons between LES and
86 experiments typically concentrate only on low-order statistics like means, variances or co-
87 variances. However, the evaluation of turbulence-resolving simulations should also assess to
88 what degree the model is able to reproduce the structure of turbulence. For this purpose, it is
89 important to compare higher-order turbulence parameters such as e.g. integral time scales,
90 spectral energy, and the scales of motions contributing to turbulent fluxes, which can be
91 determined using time-series analysis methods.

92 With this study we propose a multi-level LES validation concept for turbulent flow in
93 the near-surface atmospheric boundary layer. Instead of relying on single figures of merit,
94 the validation concept focuses on the comparative analysis of a multitude of relevant flow
95 quantities. By focusing on eddy statistics and characteristics of turbulence structures in sim-
96 ulation and experiment, the procedure specifically aims at the heart of LES: the representa-
97 tion of energy-containing eddies. We test the suitability of the proposed validation strategy
98 based on flow in a complex urban environment: the high-density urban centre of the city
99 of Hamburg, Germany. Turbulent flow is simulated with a high-resolution eddy-resolving
100 aerodynamics code based on an implicit LES approach. With respect to resolution, domain
101 size, and computing times, the code represents the advanced state-of-the-art. Reference data
102 are available from boundary-layer wind-tunnel measurements in an urban scale model.

103 In part I of this study, presented in the following, we are introducing the validation concep-
104 t (Sect. 2) and present an overview of the test case together with specifics of the LES
105 and the wind-tunnel experiment (Sect. 3). We also cover the first level of the proposed val-
106 idation strategy, the exploratory data analysis. This step focuses on comparing mean flow
107 and turbulence statistics (Sect. 4) and the underlying frequency distributions of instanta-
108 neous velocities in the horizontal plane (Sect. 5). Initial conclusions drawn from this first
109 comparisons are discussed in Sect. 6.

110 In part II we extend the validation exercise to the comparison of turbulence scales by
111 means of temporal auto-correlations and turbulence spectra and discuss comparisons based
112 on the applications of conditional resampling (quadrant analysis) and joint time frequency
113 analyses (wavelet transform).

114 2 Validation method

115 At the start of the computer revolution in fluid mechanics, Bradshaw [14] predicted a “fact
 116 gap” emerging between the capability to simulate turbulent flow in unprecedented detail and
 117 the potential to determine the accuracy of such simulations with experiments. As discussed
 118 by Oberkampf and Trucano [47], numerical and experimental approaches in engineering
 119 historically had a tendency of being competitive rather than complementary, resulting in
 120 CFD proceeding “(...) on a path that is largely independent of validation”. Similarly, Wyn-
 121 gaard and Peltier [71] stated that the coupling between experiments and modelling that has a
 122 strong tradition in micro-meteorology has been remarkably lacking in meteorological LES.

123 A model is validated in order to determine whether its combination of conceptual and
 124 computational components allow an accurate simulation of the physical problem of interest
 125 from the perspective of a specific application [1, 25, 47]. Model validation primarily depends
 126 on two essential factors: the availability of suitable reference data [37] and the application
 127 of comparison strategies for model-specific performance assessments [57, 47, 4]. Whether
 128 or not reference data are suitable strongly depends on the level of description provided by
 129 the simulation. For turbulence-resolving CFD techniques like LES, the experimental design
 130 should be suitable for the characterisation of flow structures. In an ideal scenario, the quan-
 131 tities of interest are provided with a spatial-temporal resolution that is comparable to that
 132 of the numerical output [2]. Presently, time-resolved single-point measurements and space-
 133 resolved multi-point (mostly 1D or 2D) fields of either low time resolution or restricted
 134 spatial extent represent the state-of-the-art of experiments in the field and laboratory. In the
 135 case of urban flow, using space-resolving measurement techniques like laser-based particle
 136 image velocimetry in the wind tunnel is a challenge as not all desired locations may be
 137 accessible deep within street canyons.

138 We propose a multi-level concept for the in-depth LES validation for turbulent flow
 139 in the near-surface boundary-layer based on experimental data, which is schematically il-
 140 lustrated in Fig. 1. At the “data level” we consider instantaneous, time-resolved LES flow
 141 quantities, e.g. in terms of the instantaneous velocity components $U_i^{les}(\mathbf{x}, t)$, with $i = 1, 2, 3$,
 142 which depend on the filter width Δ_i , the mesh size h_i , and the time resolution δt , as well
 143 as their experimentally resolved instantaneous counterparts, $U_i^{exp}(\mathbf{x}, t)$, with space and time
 144 resolutions, δx_i and δt , that are provided by the respective measurement technique. As an
 145 important prerequisite for a fair performance assessment the model validation should be per-
 146 formed as a blind test; neither the measurements nor the simulation should be deliberately
 147 tuned to optimise the level of agreement. This means that data exchange before running the
 148 model should be restricted to information about relevant boundary conditions of the experi-
 149 ment, enabling modellers to limit the degrees of freedom in the simulation setup.

150 The “testing level” is divided into three parts, starting with an initial exploratory data
 151 analysis through the comparison of low-order statistics. This general assessment can then be
 152 further supported by analysing the frequency distributions of the underlying instantaneous
 153 flow variables. This enables more wide-ranging conclusions to be drawn about the over-
 154 all agreement of sample characteristics. Since LES directly resolves the energy-carrying
 155 eddies of the flow, the second level focuses on a comparative analysis of eddy statistics.
 156 Based on multi-point and/or multi-time correlations, integral length/time scales as well as
 157 spatial/temporal structure functions can be derived and compared. Further insights into the
 158 structure of turbulence can also be gained from the comparison of energy-density spectra.
 159 In the third and final level of the validation, advanced methods from the field of flow pat-
 160 tern recognition are applied in order to evaluate the representation of eddy structures based
 161 on their scale statistics. Depending on the resolution properties of the data, established ap-

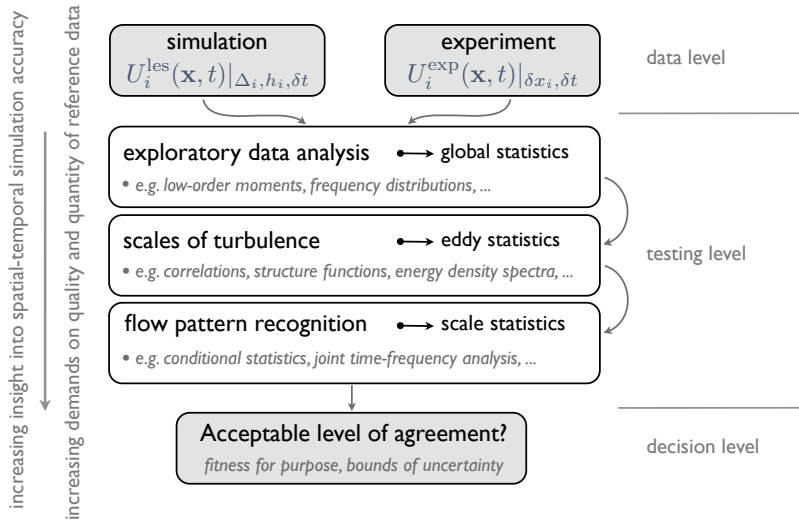


Fig. 1: Hierarchy of analysis methods for LES validation of turbulent boundary layer flow.

162 proaches based on conditional resampling (e.g. as part of quadrant analysis of turbulent
 163 fluxes), joint time-frequency analyses (e.g. using wavelet transform methods), or flow re-
 164 construction techniques, e.g. by means of empirical orthogonal functions or stochastic esti-
 165 mation [31], can be employed here.

166 Based on the outcome of these comparisons, in the final “decision level” it has to be
 167 decided whether or not the level of agreement between simulation and reference data is suf-
 168 ficient and hence if the model is acceptable for its intended application. If the answer is
 169 negative, the findings from the testing level should be used to determine necessary improve-
 170 ments to the model and the testing has to be repeated until the desired level of agreement
 171 is achieved. Whether or not the simulation quality is deemed sufficient and what deviations
 172 from the experiment are considered acceptable, strongly depends on the intended use of
 173 the model and possible consequences related to the margins of uncertainty of the simula-
 174 tion. In validation studies of steady-state CFD-RANS models it is common practice to base
 175 the decision about the quality of the model on one-dimensional statistical measures known
 176 as validation metrics, e.g. [16]. By defining acceptable, application-specific thresholds for
 177 these metrics the model performance can be judged and easily compared with other models.
 178 This approach can be employed as part of the exploratory data analysis proposed above.
 179 However, validation metrics do not offer direct physical insight and inferring information
 180 about reasons for accuracy limitations is difficult. Therefore it is generally recommended
 181 to use these measures in combination with detailed point-by-point analyses. Such detailed
 182 comparisons can for example focus on questions like: *Are space/time patterns or trends in*
 183 *the variables of interest reproduced by the LES? Are flow features captured that are impor-*
 184 *tant for the problem under study? Do general conclusions about the physical state of the*
 185 *flow in the LES agree with the experiment?* In practice the corresponding qualitative and
 186 quantitative information can for example be based on height profiles of the variables of in-
 187 terest, on comparisons of histograms or of time-lag or frequency dependent statistics. The

188 LES results from the validation test case presented in the following will be assessed along
189 these lines.

190 3 Test case, experiment and simulation

191 The validation method is applied to the case of isothermal urban flow in the city of Hamburg,
192 Germany, for which high-resolution LES data and comprehensive boundary-layer wind-
193 tunnel data were generated. Fig. 2 shows the regions covered by the computational and
194 experimental domains, respectively. Information about the urban test environment, the lab-
195 oratory experiment and the LES are presented in the following sections.

196 3.1 Urban test environment

197 The domain of interest is centered on the inner city area of Hamburg. The Elbe river sep-
198 arates the industrial harbour area to the south, mainly featuring low-story storage build-
199 ings and production facilities, from the inner-city district to the north that is characterised
200 by high-rise, high-density building structure. The urban morphology of the inner city cor-
201 responds to typical northern and central European cities with closely packed, heteroge-
202 neously shaped buildings of similar heights, narrow street canyons and complex intersec-
203 tions. Based on the buildings included in the wind-tunnel domain, an average building height
204 of $H = 34.3$ m is obtained for the district north of the Elbe. Here, typical street canyon
205 widths are in the order of $W = 20$ m, with individual street widths between 10 m and 50 m.
206 The typical street-canyon aspect ratio in the inner city is $H/W = 1.72$, with individual val-
207 ues ranging between 0.7 and > 3 . This implies the dominance of skimming flow regimes,
208 while in the presence of open spaces or wide intersections chaotic wake-interference flow
209 is prevailing [24,40]. In the industrial area on the southern shore of the river, the average
210 building height is much lower with an average of about 21 m and isolated roughness flow is
211 prevailing.

212 3.1.1 Flow comparison sites

213 Overall 22 sites distributed across the inner city were selected for the validation exercise in
214 order to cover a wide range of typical UCL flow features and investigate the influence of
215 changes in the underlying city structure on roughness-sublayer flow. Data are mostly avail-
216 able in terms of densely spaced vertical profiles, allowing the investigation of the height-
217 dependent structure of the flow and vertical momentum exchange. Fig. 3 shows the positions
218 of the flow comparison sites. Locations marked by the prefix “BL” are distributed at various
219 downstream positions within the gradually increasing internal boundary layer forming after
220 the roughness change from the industrial harbour region to the inner city, which are sepa-
221 rated by the Elbe river. The “RM” locations are closely distributed around the city hall. This
222 area is interesting due to its diverse building geometry. Within the “DM” area, reference
223 measurements were carried out with a higher horizontal resolution in order to resolve the
224 flow field at a courtyard entrance. Based on this sample of comparison sites it is possible to
225 assess whether the LES is able to capture important flow features like wake recirculation in
226 cross-wind canyons (BL11), helical motions in canyons oriented at oblique angles (BL12),
227 flow channelling in along-wind canyons (RM07), flow through geometrically confined open
228 spaces (e.g. BL08, BL10, RM10, RM09), intersection flow (RM03, BL10), stagnating flow

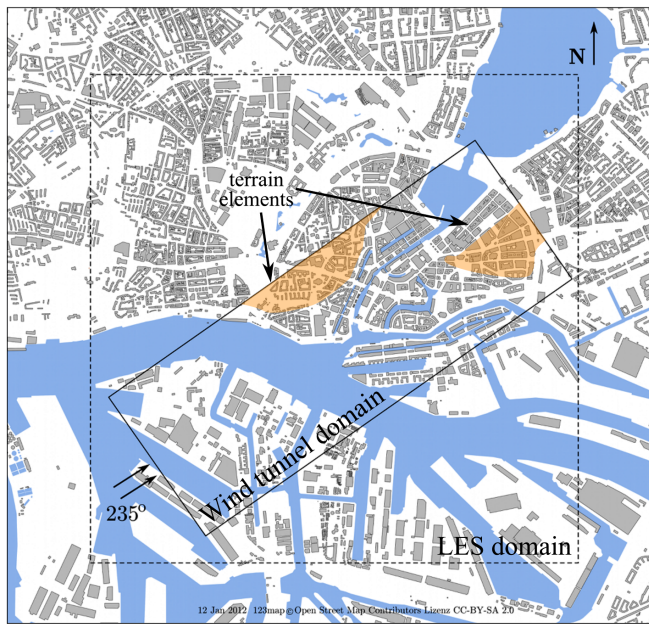


Fig. 2: Experimental and computational domains covering the inner city of Hamburg. Solid rectangle: $1.4 \text{ km} \times 3.7 \text{ km}$ wind-tunnel model area; dashed square: $4 \text{ km} \times 4 \text{ km}$ computational domain for the LES. The areas in which terrain is relevant and therefore included in the wind-tunnel scale model are indicated as well. The maximum offsets to ground level are 20 m (terrain to the west) and 7 m (terrain to the east).

229 on the windward side of a building (BL07) and flow into and within courtyards (DM, BL09).
 230 Capturing such flow features is essential for an accurate simulation of scalar dispersion in
 231 cities regarding both the mean plume structure and local, time-dependent concentration fluc-
 232 tuations. The unobstructed site BL04 above the Elbe river is representative of the approach
 233 flow conditions upstream of city centre in LES and experiment and used as a flow reference
 234 location (see Sect. 3.2.2).

235 3.2 Wind-tunnel experiment

236 Flow experiments were conducted in the open-circuit boundary-layer wind tunnel WOTAN
 237 of the Environmental Wind Tunnel Laboratory (EWTL) at the University of Hamburg. With
 238 a test section of 18 m in length, 4 m in width and a ceiling of adjustable height between
 239 2.75 m and 3.25 m, WOTAN is one of the largest low-speed, suction-type wind tunnel
 240 facilities worldwide for the physical modelling of isothermal boundary layers.

241 Information about buildings, terrain elevations and outlines of bodies of water in central
 242 Hamburg was provided by the Hamburg geo-information service. Detailed 3D building data
 243 was available at a minimum resolution of 0.5 m. The wind-tunnel model was built at a scale
 244 of 1:350, reproducing all relevant buildings down to 0.5 m full scale (approx. 1.5 mm in
 245 model scale). The longitudinal/lateral extents of the model area were 3.7 km/1.4 km full-
 246 scale (10.5 m/4 m model scale). Rolling terrain was reproduced by stacking layers of thin

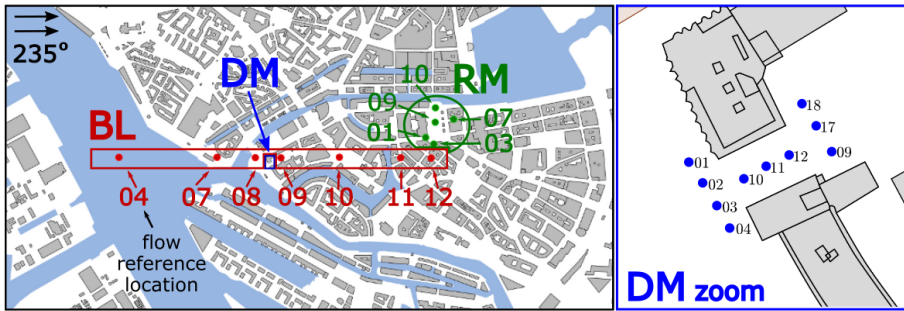


Fig. 3: Left: wind-tunnel model area indicating locations and IDs of the flow comparison sites: boundary-layer development positions (prefix BL, red dots), sites around the city hall (prefix RM, green dots), and the dense measurement site at a courtyard entrance (DM, blue rectangle). Right: exact locations of the 10 DM sites.

247 wooden plates, each having a depth of 2 mm in model scale equating to offsets of 0.7 m in
 248 the field (areas indicated in Fig. 2). The water level of the Elbe river and city canals was
 249 represented as being close to high tide, resulting in a full-scale vertical offset of 3.5 m to
 250 land (1 cm in model scale). The most significant abstraction of the scale model is given by
 251 neglecting all types of urban vegetation, smaller bridges and traffic overpasses. The model
 252 orientation with the ambient flow approaching from the south-west (235°) represents a pre-
 253 dominant meteorological situation for the city. Fig. 4 shows the inner city area as viewed
 254 from 235° (south-west) and 35° (north-east) together with corresponding views in the labo-
 255 ratory.

256 3.2.1 Inflow specifications and modelling

257 Properly chosen flow boundary conditions in the reference experiment are vital for model
 258 validation. Specifying appropriate inflow boundary conditions is not a trivial task, especially
 259 when investigating flow in urban areas.

260 As a guidance for the generation of realistic inflow conditions for both the wind-tunnel
 261 model and the LES, information about vertical mean flow and turbulence profiles were de-
 262 rived from meteorological tower measurements [68]. The tower is situated in a suburban
 263 setting about 8 km south-east of the study domain. *In-situ* sonic anemometer measurements
 264 of all three velocity components and temperature were available at five measurement heights
 265 (10 m, 50 m, 110 m, 175 m and 250 m) at resolutions of 10 and 20 Hz. Detailed information
 266 about the facility and local climatology are presented by Konow [36]. An in-depth descrip-
 267 tion of the field data analysis for the validation test case is presented by Hertwig [29]. For
 268 the sake of brevity only the main findings are summarised here.

269 Based on a three year data record (2007–2009) the roughness length z_0 and the power-
 270 law wind profile exponent α were derived for flow approaching the tower from a sector
 271 of $235^\circ \pm 30^\circ$ under neutral stability conditions. Within this sector, the surface roughness
 272 characteristics are very homogeneous with mixed land use and low-density industrial zones,
 273 frequently loosened by side branches of the Elbe river. Structurally this is comparable to the
 274 situation in the inflow corridor for the wind-tunnel model, although the latter is expected to
 275 be rougher due to the harbour industry. z_0 was found to be of order $1.2 \text{ m} \pm 0.24 \text{ m}$, whereas
 276 α was 0.29 ± 0.01 based on a reference height of 175 m. This reference height was found to



Fig. 4: Aerial photographs of the central part of the Hamburg domain together with the representation in the wind-tunnel model. Left: view from the south-west towards the inner city area. Right: view from the north-east towards the industrial harbour.

277 be representative of the depth of the surface layer (constant flux layer) for neutral stability
 278 conditions and mean wind speeds higher than 1 m s^{-1} . For the derivation of turbulence
 279 intensities, spectral energy densities, and integral length scales the data was analysed over
 280 periods of negligible synoptic trends.

281 These characteristics were used as benchmarks for the physical modelling process in
 282 the wind tunnel. In addition, the generated laboratory boundary layer characteristics were
 283 in agreement with wind-tunnel modelling guidelines and established standards, e.g. [23,
 284 66]. At the tunnel entrance an array of 7 flat vortex generators with triangular front faces
 285 was mounted (modified Standen spires [59]). The subsequent 7.2 m long flow development
 286 section was covered with 25 rows of floor roughness elements (sharp-edged metal brackets)
 287 arranged in a staggered array to generate realistic suburban/urban roughness conditions. It
 288 was experimentally verified that stationary and horizontally homogeneous flow conditions
 289 were established at the end of the development section just upstream of the urban model.

290 Fig. 5 shows that vertical profiles of mean streamwise velocities, turbulence intensities
 291 and turbulence integral length scales derived from the field measurements and the wind-
 292 tunnel approach flow are in good agreement. Overall the wind tunnel approach flow corre-
 293 sponds to a rougher surface type ($z_{0WT} = 2 \text{ m} \pm 0.67 \text{ m}$ with $\alpha_{WT} = 0.29 \pm 0.01$). This trend
 294 is also seen in the turbulence intensities based on the spanwise and vertical velocity compo-
 295 nents (not shown). The rougher surface characteristics of the wind-tunnel flow are expected
 296 to better represent the actual flow situation in the presence of the industrial harbour, which
 297 starts approximately 4 km upstream of the domain inflow edge. This feature is not seen by
 298 the field site sensors for the same south-westerly approach flow direction.

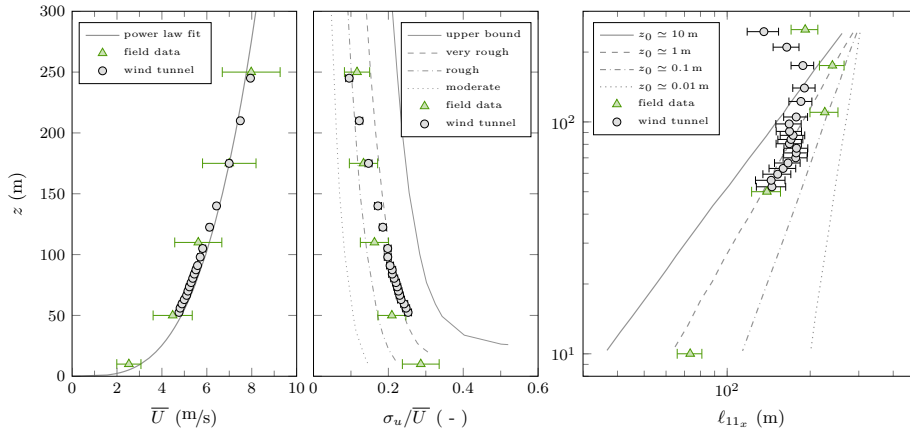


Fig. 5: Comparison of field (triangles) and wind tunnel (dots) vertical profiles in the approach flow boundary layer. Left: mean streamwise velocity together with a power-law fit for $\alpha = 0.29$. Centre: turbulence intensity of the streamwise velocity with empirical boundaries for different roughness regimes according to ESDU [23]. Right: turbulence integral length scales in longitudinal direction derived from streamwise velocities. Lines indicate empirical boundaries of different roughness regimes following Counihan [20].

3.2.2 Flow measurements

Schematics of the wind tunnel model area and of the flow measurement set-up are presented in Fig. 6. The free-stream velocity was $U_\infty \simeq 10 \text{ m s}^{-1}$ to ensure Reynolds number independence. This was tested over a wide range of velocities, with the selected U_∞ being on the safe side even when measuring in narrow urban street canyons. In order to guarantee Re -independence close to solid boundaries, model buildings and ground plates all had aerodynamically rough surfaces. The characteristic flow Reynolds number in the test section was $Re \simeq 2.67 \cdot 10^6$ based on U_∞ and a length scale of 4 m (tunnel width). Within the urban scale model this corresponds to $Re_H = 2.97 \cdot 10^4$ based on the average inner city building height H and a typical velocity at this height of $U_H \simeq 4.55 \text{ m s}^{-1}$, which was determined at the end of the flow development section. Re_H complies well with established criteria for the reliable physical modelling of urban flows, as outlined for example by Plate [52]. The wind-tunnel measurement sites shown in Fig. 3 were located in sufficient distance to lateral and outflow boundaries of the tunnel to ensure that the local flow field at these sites is neither affected by boundary layers forming at the tunnel side-walls or by the open outflow at the end of the test section.

Single-point high-resolution velocity records were acquired with a two-component fibre-optic Dantec laser Doppler anemometry (LDA) system. The LDA was operated to simultaneously measure the streamwise and vertical velocities (U - W mode) and the streamwise and spanwise velocities (U - V mode) using laser beams with wavelengths of 514.5 nm and 488 nm. With a focal length of 160 mm and an initial beam separation of 15 mm the LDA measuring volume had a diameter of 0.08 mm and a length of 1.6 mm. Haze-droplets with diameters of 1–2 μm emitted by a commercial-grade hazer were used to seed the flow. The LDA probe was moved by an automated 3D traverse system. The average LDA sampling frequencies (mean data rates \dot{N}) depend on local seeding conditions within the model do-

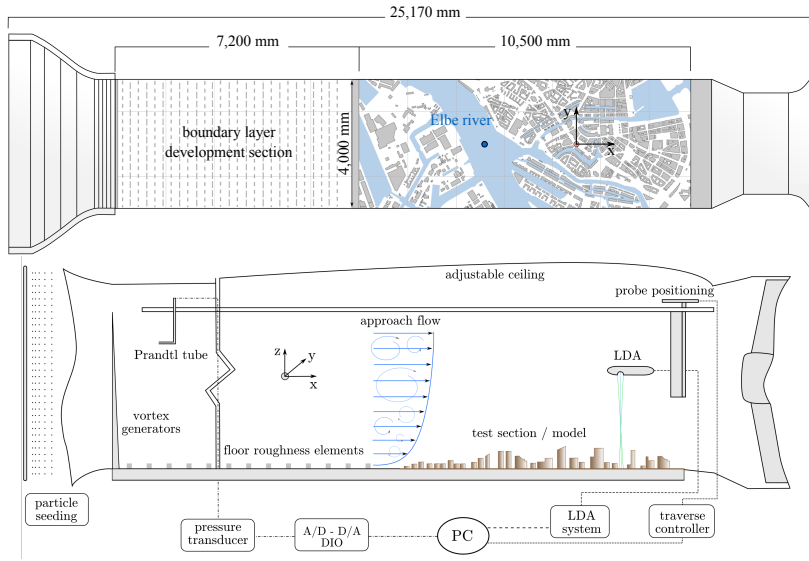


Fig. 6: Top: plan-view of the boundary-layer wind tunnel WOTAN. The red dot marks the coordinate origin and the flow reference location above the Elbe river is indicated by the blue dot. Bottom: side-view of the measurement set-up with the LDA probe aligned in U - V mode. Note that distances and heights are not true to scale. The flow is approaching from the left.

324 main and were typically in the order of 50 Hz (locations with low wind speeds) to 600 Hz
 325 (high wind speeds). Time series were recorded for 170 s to minimise the inherent uncer-
 326 tainty in derived statistics and enable representative analyses of large eddy structures. The
 327 measurement duration was determined from statistical convergence tests conducted at various
 328 flow locations. Taking into account the geometric scale of 1:350 this corresponds to a
 329 full-scale measurement duration of about 16.5 h at the same reference velocity.

330 A pitot-static tube was operated together with the LDA to record the free-stream velocity
 331 U_∞ in the tunnel during each measurement run. The pitot-tube signal was recorded by a
 332 pressure transducer delivering voltage signals to an analog-to-digital converter. All LDA-
 333 measured velocities and derived quantities are referenced to U_{ref} corresponding to the mean
 334 streamwise velocity at a height of $z_{ref} = 49$ m above the Elbe river (i.e. 45.5m or 1.33H
 335 above ground level; see Fig. 6).

336 3.2.3 LDA signal resampling

337 By nature, LDA provides discontinuous flow information. The time step between detected
 338 velocity signals is not uniform since seeding particles pass the measuring volume at random
 339 intervals. For time-series analyses in this study, the discontinuous time records are resampled
 340 to a new constant time step δt_r given by the inverse of the mean data rate \dot{N} . We reconstruct
 341 the LDA signals by using a 0th order polynomial interpolation, known in signal-processing
 342 as sample-and-hold technique (S&H) [22].

343 Fig. 7 shows frequency distributions of streamwise velocity fluctuations obtained from
 344 the raw LDA data and the corresponding S&H signal interpolation together with results

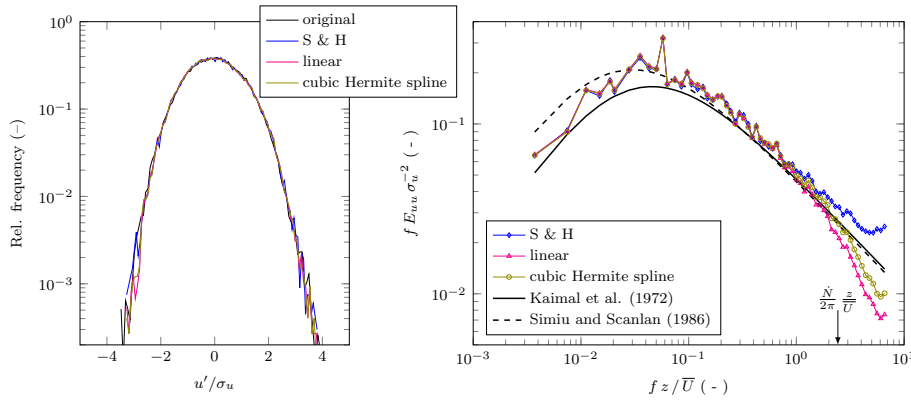


Fig. 7: Quality assessment of reconstructed LDA signals based on an example time series taken at a full-scale height of $z = 45.5$ m with a mean data rate of $\dot{N} = 551$ Hz. Left: normalised frequency distributions of the streamwise velocity fluctuations. Right: 1D energy density spectra of the streamwise velocity. The arrow indicates the empirical upper limit of validity of the S&H spectrum according to Adrian and Yao [3].

345 for higher-order reconstructions using linear and cubic Hermite spline interpolations. With
 346 all techniques the original distribution is very well recovered. This is also evident from
 347 the corresponding 1D energy density spectra in comparison to reference spectra [33,58].
 348 However, both the linear and cubic Hermite curves show an increased energy roll-off at
 349 high frequencies, which could be mistaken as the onset of the dissipation range. The S&H
 350 estimate follows the expected $-2/3$ slope slightly longer, but shows an enhanced spectral
 351 aliasing effect. As discussed by Adrian and Yao [3], S&H affects the spectrum through
 352 additive step-noise caused by the holding mechanism, whose contribution diminishes for
 353 high data rates with \dot{N}^{-3} and, secondly, through a low-pass filter with a cut-off frequency
 354 at $\dot{N}/(2\pi)$. This designates the upper limit of an unbiased spectral estimate (see arrow in
 355 Fig. 7). However, in the low-frequency range, which can be resolved directly with LES,
 356 the interpolation techniques provide reliable estimates. Simple S&H performs equally well as
 357 linear and cubic reconstructions and was selected as the method of choice in this study due
 358 to its robustness and assessable statistical bias [3,70], which is less well-explored for the
 359 other approaches [21,53].

360 3.3 Large-eddy simulation

361 Turbulence-resolving CFD computations were conducted with the urban aerodynamics LES
 362 code FAST3D-CT that is developed and operated by the U.S. Naval Research Laboratory.
 363 The model is based on a monotone integrated large-eddy simulation (MILES) methodology
 364 [8, 11] that handles dynamical effects of sub-grid scales implicitly through numerical diffu-
 365 sion using the flux-corrected transport (FCT) approach [12, 13, 7, 5]. Relevant physics and
 366 numerics within FAST3D-CT are discussed in detail by Patnaik et al. [51,50].

367 3D flow simulations were performed in a $4 \text{ km} \times 4 \text{ km}$ computational domain encom-
 368 passing the inner city of Hamburg (Fig. 2). The computations were conducted on a structured
 369 Cartesian grid with a uniform resolution of 2.5 m up to a height of 101.5 m above ground

370 (approx. $3H$; corresponding to the lowest 42 grid cells). From there on the grid was gradu-
371 ally stretched vertically up to the domain top at 1.4 km. Overall the computational domain
372 was covered by $1,600 \times 1,600 \times 80$ grid cells in x, y, z directions.

373 Buildings were represented by using simple grid masking. In order to avoid very steep
374 vertical gradients at the surface, rolling terrain was represented with a much smoother
375 shaved-cell approach. While the masking procedure is computationally efficient, it leads
376 to a staggering of surfaces (“staircase effects”), for example for slanted roofs or building
377 oriented at oblique angles within the grid. This needs to be kept in mind when comparing
378 local flow features to the wind-tunnel measurements that were conducted in a model of much
379 higher geometric resolution. As in the laboratory model, urban vegetation, bridges, traffic
380 overpasses and passages through buildings or openings to indoor areas were not reproduced.

381 Turbulent, time-dependent inflow boundary conditions were generated at each time-step
382 by using an imposed fluctuation method. Artificially generated, deterministic turbulent fluctu-
383 ations are superimposed on mean flow profiles that are based on information from the
384 wind-tunnel approach flow. The non-periodic velocity fluctuations were constructed from
385 a non-linear superposition of different fluctuation wavelengths and amplitudes (see [10,51]
386 for details). At the bottom of the domain a rough-wall boundary layer model is used to rep-
387 resent wall shear stresses. At the domain top and at the lateral boundaries extra layers of
388 cells were implemented to act as a buffer between the self-consistent simulation and the
389 analytically prescribed boundary constraints. Here, an inflow-outflow algorithm is used that
390 changes continuously from the analytical inflow specification described above to a simple
391 extrapolation for an open outflow [10].

392 The simulation ran for 7 weeks on an SGI Altix computer with 64 CPUs, using a com-
393 putational time step of 0.05 s at a velocity of approximately 7 m s^{-1} at 200 m above ground.
394 Velocity signals were extracted at cell centres every 0.5 s of real time over a duration of
395 23,250 s (approx. 6.5 h). The geometric and physical complexity of the model was as close
396 as possible to that of the experiment. As in the laboratory, the mean inflow wind direction
397 was from 235° and the atmospheric stratification was set to neutral. The characteristic flow
398 Reynolds number for the LES was $Re \simeq 1.12 \cdot 10^9$ based on the domain depth of 1.4 km and
399 a velocity of 12 m s^{-1} at that height, whereas Re_H was $9.72 \cdot 10^6$.

400 The approaching LES boundary-layer flow was compared to the wind-tunnel conditions
401 at the flow reference location above the river upstream of the inner city (site BL04; Fig. 3),
402 allowing enough fetch for the simulation to reach a “self-contained” state. Within the rough-
403 ness sublayer profiles of mean flow and turbulence statistics were in very good quantitative
404 agreement with the experiment. Comparing energy-density spectra, however, revealed that
405 above $1H$ the artificial inflow turbulence prescribed at the inlet still left a footprint in the flow
406 structure. In particular, this showed in LES spectral energy peaks being located at higher
407 frequencies (i.e. smaller eddies scales) than their wind-tunnel counterparts. Further down-
408 stream within and above the city these effects were “washed out”, indicating an increase in
409 physical quality of the simulation in response to real obstacle-induced turbulence.

410 The specific purpose of the simulation with FAST3D-CT was the provision of flow data
411 for the use in the emergency response plume model CT-Analyst, a tool that can be used
412 for fast predictions of the dispersion of air-borne contaminants from localised releases in
413 cities [9,6]. For this purpose the LES data is processed to derive mean-flow statistics and
414 local velocity fluctuation characteristics, from which typical urban dispersion pathways are
415 extrapolated in the lower roughness sublayer (up to an elevation of $2H$). The validation
416 effort, therefore, is focused on determining whether building-induced turbulence and ex-
417 change processes are simulated accurately. An in-depth investigation of time series can help
418 to reveal sources of inaccuracy that may not show in low-order statistics (e.g. through error

419 cancellation) and enables a deeper understanding of strengths and limitations of the model,
 420 also with a view to other types of applications.

421 **4 Mean flow features**

422 In this section results of the first testing level of the LES validation scheme (Fig. 1) are pre-
 423 sented using a fixed Cartesian model coordinate system (x, y, z) as indicated in Fig. 6. The
 424 corresponding streamwise, spanwise and vertical components U_i ($i = 1, 2, 3$) of the veloc-
 425 ity vector are denoted as U , V and W . Overbars denote time-averaged quantities. Velocity
 426 statistics are presented in a dimensionless framework based on the mean streamwise refer-
 427 ence velocity U_{ref} (Sect. 3.2.2).

428 Data from the LES were extracted at cell centres and associated with the wind-tunnel
 429 measurement points based on a nearest neighbour pairing, i.e. the simulation results were
 430 not spatially interpolated to the locations of the wind-tunnel measurements points. This ap-
 431 proach can result in horizontal and vertical offsets between the data pairs. These offsets,
 432 however, are mostly in the order of the spatial accuracy of the LDA measurement tech-
 433 nique, which is dominated by the extent of the measuring volume along its principle axis
 434 of 1.6 mm, corresponding to 0.56 m in full scale taking into account the model scale of
 435 1:350 (Sect. 3.2.2). In U - V mode, the principle axis is aligned with the vertical z -axis and
 436 in U - W mode with the lateral y -axis. These spatial resolution aspects of the LDA need to be
 437 considered particularly in flow regions with strong velocity gradients.

438 In the following paragraphs and in Sect. 5, only a fraction of the comparison results can
 439 be discussed in detail. The results presented here were selected in order to cover a variety of
 440 different flow scenarios at sites that were indicative of strengths and limitations of the model.
 441 The selection is representative of the overall agreement between experiment and LES.

442 **4.1 Vertical flow profiles**

443 Height profiles of mean flow and turbulence statistics derived from the horizontal velocity
 444 components are compared in Fig. 8 at four locations covering different geometry-induced
 445 flow scenarios: relatively unobstructed flow just downstream of the river (BL07); flow in
 446 a spanwise street canyon oriented at approx. 45° from inflow direction (BL12; canyon
 447 width approx. 13.5 m), intersection flow (RM03) and flow channelling through a streamwise
 448 canyon (RM07; canyon width approx. 14 m). From the wind-tunnel studies, densely spaced
 449 vertical velocity profiles are available covering the roughness sublayer up to approximately
 450 $2H$, enabling an application-specific validation of the urban aerodynamics code.

451 Scatter bars for the wind-tunnel values are based on the reproducibility of experimen-
 452 tal flow statistics, assessed through a series of repetition measurements at different heights
 453 within the urban boundary layer. For this, vertical velocity profiles were taken repeatedly at
 454 two locations: site BL07 for U - V measurements and in the wind-tunnel approach flow for
 455 U - W measurements in order to have a better data coverage at low heights. For each mea-
 456 surement location, the run-to-run scatter of flow statistics at different measurement heights
 457 was determined. In order to provide a conservative estimate, the reproducibility was then
 458 based on the maximum value range determined over all heights for the specific statistical
 459 quantity of interest. For \bar{U}/U_{ref} the statistical scatter was found to be ± 0.0185 , for \bar{V}/U_{ref}
 460 ± 0.0204 and for $\sigma_v^2/U_{ref}^2 \pm 0.0027$.

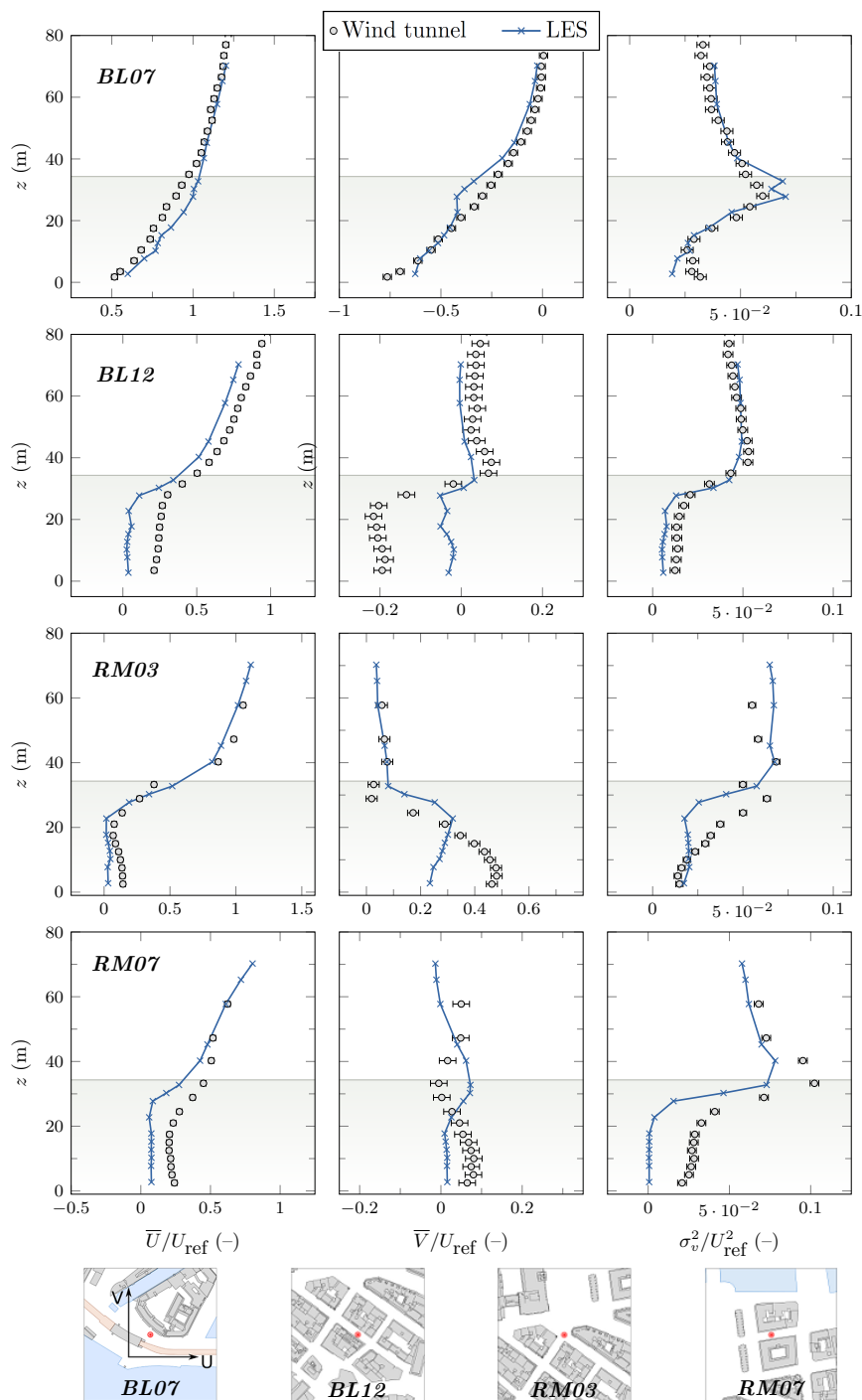


Fig. 8: Comparison of height profiles of means and variances of the horizontal velocity components at different locations within the inner city area (wind tunnel: dots; LES: crosses). The grey shading indicates heights lower than the mean building height of $H = 34.3$ m. Maps showing the location of the comparison points depict an area of $210 \text{ m} \times 210 \text{ m}$.

461 The results presented here are characteristic for the overall level determined from the
 462 entire ensemble of comparison sites. Overall, the LES captures the general qualitative trends
 463 of the horizontal mean velocities and variances with height at most of the locations. This, for
 464 example, can be seen in the agreement of characteristic peak heights of flow variables at the
 465 top of the canopy layer. However, for some of the positions, particularly those characterised
 466 by a strong topological confinement of the flow, the quantitative discrepancies are larger
 467 for some of the variables compared. Here, the LES shows a systematic trend of under-
 468 predicting mean velocities (BL12) and variances (RM07) in the canopy layer. For these
 469 two street-canyon locations the ratio of canyon width to LES grid spacing, W/h_i , is of order
 470 5.5. In combination with the “staircase effects” caused by the gridding technique the spatial
 471 resolution of 2.5 m in the LES is probably too low to reliably resolve the flow at these points.
 472 The relatively coarser representation of buildings in the LES could have caused some of
 473 the profile locations to effectively move closer to the building walls, which increases the
 474 influence of the prescribed wall-boundary condition on the extracted results.

475 4.2 Validation metrics

476 The above comparisons showed that the LES is able to represent, to a reasonable degree,
 477 complex urban flow pattern emerging in the roughness sublayer on the mean level at dif-
 478 ferent comparison locations while locally showing trends towards an under-prediction of
 479 velocity magnitudes. As recommended for the validation of RANS-based simulations, the
 480 exploratory data analysis can be extended into a more quantitative comparison using suitable
 481 validation metrics [46, 16]. Fig. 9 depicts scatter plots of wind tunnel against LES results of
 482 horizontal velocity statistics, showing overall 135 experimental and numerical data pairs at
 483 locations that can be directly compared due to comparatively small spatial offsets. The max-
 484 imum offset was slightly over 1 m in vertical direction affecting 10 data pairs at the DM site.
 485 The majority of scatter points fall well within the margins given by a 1:2 and 2:1 relationship
 486 between experiment and simulation. The agreement is further quantified in the next step.

487 From the large variety of available validation metrics, see e.g. [28, 16, 26], we have se-
 488 lected a choice of the most common methods (Eqs. 1–4) to assess: (1) the overall perfor-
 489 mance of the model with some robustness to infrequently occurring strong over-predictions
 490 or under-predictions (i.e. $FAC2$, although $FAC5$ is routinely considered as well), (2) the
 491 tendency of the model to over/under-predict ($MNMB$), (3) the mean absolute error of the
 492 simulation (FGE), and (4) the degree of common variation (i.e. trends) in both datasets
 493 based on the linear correlation coefficient R .

494 1. Factor of two:

$$FAC2 = \frac{1}{N} \sum_i F_i \text{ with } F_i = \begin{cases} 1, & \text{if } \frac{1}{2} \leq \frac{P_i}{M_i} \leq 2 \\ 0, & \text{otherwise} \end{cases} \quad (1)$$

495 2. Modified normalised mean bias:

$$MNMB = \frac{2}{N} \sum_i \left(\frac{P_i - M_i}{P_i + M_i} \right) \quad (2)$$

496 3. Fractional gross error:

$$FGE = \frac{2}{N} \sum_i \left| \frac{P_i - M_i}{P_i + M_i} \right| \quad (3)$$

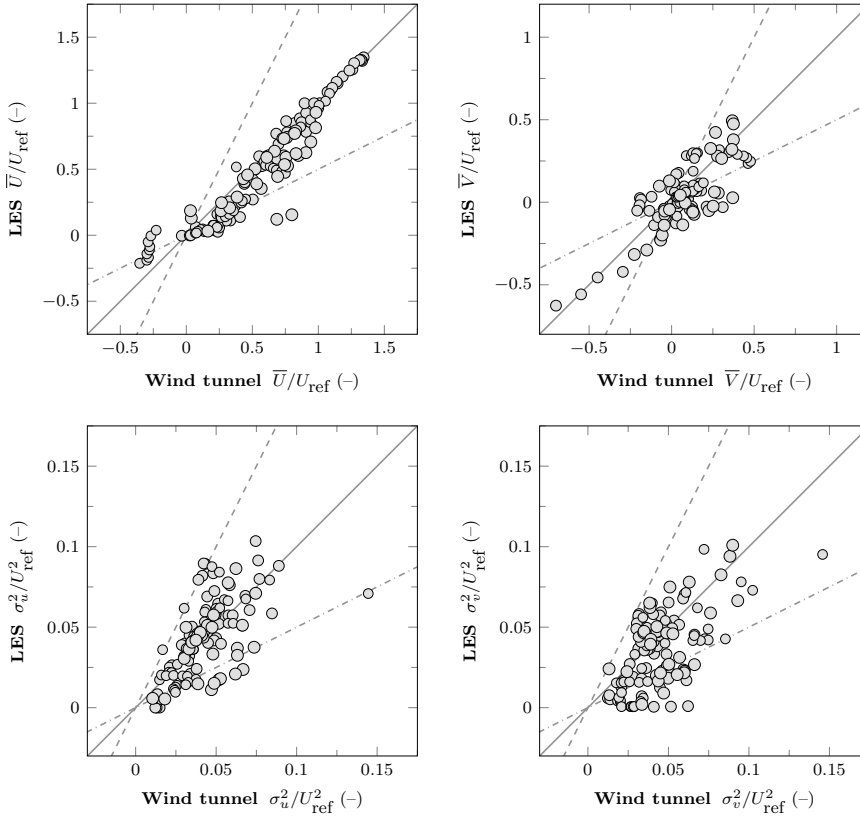


Fig. 9: Scatter plots of wind-tunnel measurements and LES results of horizontal flow statistics \bar{U}/U_{ref} , \bar{V}/U_{ref} , σ_u^2/U_{ref}^2 , and σ_v^2/U_{ref}^2 , comprising overall 135 data pairs at 22 comparison sites. Lines indicate the ideal 1:1 relationship and the factor-of-2 margins.

497 4. Correlation coefficient:

$$R = \frac{\frac{1}{N} \sum_i (P_i - \bar{P})(M_i - \bar{M})}{\sigma_P \sigma_M} \quad (4)$$

498 Here, P denotes the predicted and M the measured value, and the index $i = 1, \dots, N$ refers
 499 to one of the overall N locations at which statistics are compared. *FAC2* measures the frac-
 500 tion of LES predictions that are within a factor of two of the corresponding measurement.
 501 The simulation bias is assessed by the *MNMB*, which is bounded on the interval $[-2, +2]$.
 502 The overall mean error of the simulation can be assessed by the *FGE*, which is bounded
 503 on the interval $[0, +2]$. Both, *MNMB* and *FGE*, for which a value of 0 would correspond
 504 to a perfect prediction, treat trends of over-predictions and under-predictions symmetrically
 505 without over-emphasising outliers. Correlation coefficients, R , are consulted to quantify to
 506 whether the same data trends and patterns are seen in the measurements and the LES. In the
 507 computation of these validation metrics, the reproducibility of the experimental reference
 508 statistics was taken into account as recommended by the COST Action 732 [56].

509 The validation metrics are presented in Table 1. For all quantities *FAC2* is above 0.5
 510 indicating that typically more than half of the predictions are within a factor of two of

Table 1: Validation metrics derived for data pairs of horizontal flow statistics (Fig. 9).

	\bar{U}/U_{ref}	\bar{V}/U_{ref}	\bar{U}_h/U_{ref}	σ_u^2/U_{ref}^2	σ_v^2/U_{ref}^2
<i>FAC2</i>	0.74	0.52	0.83	0.86	0.77
<i>MNMB</i>	-0.40	0.09	-0.28	-0.11	-0.36
<i>FGE</i>	0.44	1.5	0.32	0.32	0.49
<i>R</i>	0.95	0.80	0.94	0.65	0.62

511 the observations. For dispersion studies in urban areas, this 50% threshold is often recom-
512 mended for a binary classification of the model skill into sufficient or insufficient, e.g. [28,
513 18]. More, recently this has been relaxed to 30% in the discussion of acceptance criteria
514 for urban dispersion models by Hanna and Chang [26]. However, these and other studies
515 showed assessments based on single figures of merit should be avoided and further metrics
516 need to be consulted to obtain a clear picture. The negative normalised bias values (*MNMB*)
517 indicate that the LES has a tendency to under-predict. The very good *MNMB* for \bar{V}/U_{ref} ,
518 however, is a result of the cancelling of over-predictions and under-predictions, which can be
519 seen very well in the corresponding scatter plot (Fig. 9) in the quite symmetric distribution
520 of values about the 1:1 line at small magnitudes of \bar{V}/U_{ref} . Consulting the respective *FGE*
521 value, which is based on the absolute difference between data pairs, shows that the predic-
522 tive skill of the model for this velocity component is poor. This was already indicated by the
523 comparatively low *FAC2* of 0.52. However, comparing the corresponding horizontal wind
524 speeds, $U_h = \sqrt{U^2 + V^2}$, which are independent of the selected coordinate system represen-
525 tation, results in a significantly higher level of agreement than when looking at the velocity
526 components individually. For the other quantities, the *FGE* indicates a good predictive skill
527 of the LES. The correlation coefficients indicate a high to moderate linear correspondence
528 of data sets. However, the high *R* value of 0.80 for \bar{V}/U_{ref} clearly is not representative of
529 the actual skill of the code in capturing this component, particularly at flow locations that
530 are characterised by a strong confinement of flow paths as discussed above.

531 5 Instantaneous flow features

532 5.1 Frequency distributions

533 In a next step, frequency distributions of instantaneous horizontal velocities and their corre-
534 sponding shape and spread parameters are compared.

535 Fig. 10 shows meteorological wind rose diagrams constructed from wind tunnel and
536 LES time series of instantaneous horizontal wind speeds, U_h , and horizontal directions, U_d ,
537 at three heights within a narrow street cross-wind canyon (BL11; $W = 17.5$ m), together
538 with corresponding vertical profiles. At the first comparison level ($z_{exp} = 17.5$ m), the wind
539 roses indicate opposing flow channelling directions in the experiment and LES, with the
540 latter significantly under-predicting velocity magnitudes. This is mainly caused by a flawed
541 representation of the V component. The shapes of both distributions, however, are similar in
542 that both exhibit a slight bimodal pattern. Having regard to the narrow width of the canyon,
543 the LES grid resolution seems insufficient to adequately resolve the flow at this site. As dis-
544 cussed above, this problem is reinforced by the gridding technique that can result in a further
545 virtual reduction of the width of the canyon. Hence, in the LES the comparison point can
546 be much closer to the building façade as in the experiment. At the second comparison level

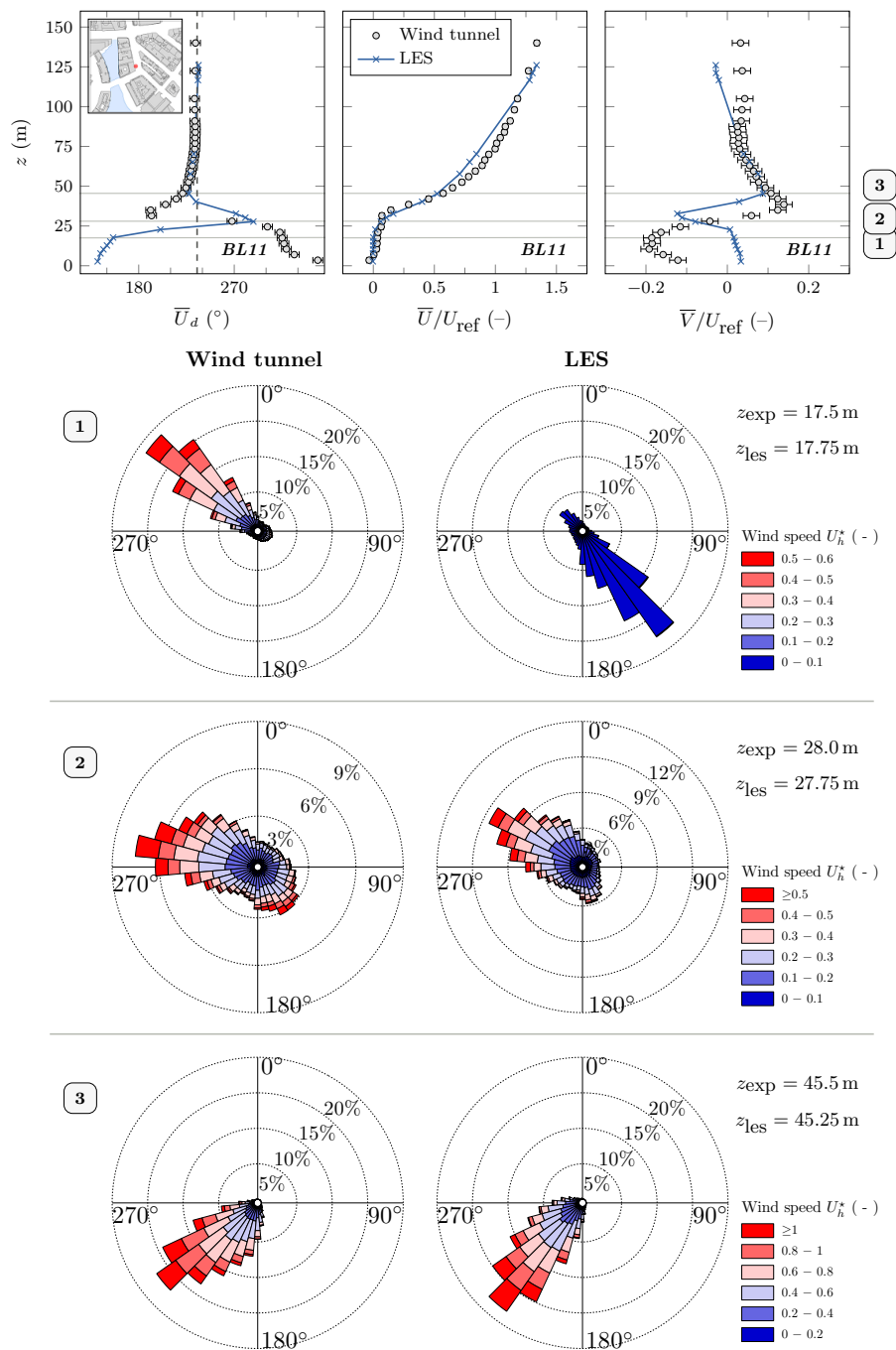


Fig. 10: Wind rose diagrams of the instantaneous horizontal wind speeds U_h/U_{ref} at three heights within and above a narrow street canyon (site BL11) for the wind tunnel (left) and the LES (right). Vertical profiles of the horizontal wind direction, U_d , and both horizontal mean velocities are shown for reference at the top (wind tunnel: dots; LES: crosses).

($z_{exp} = 28$ m), this effect is significantly mitigated and the LES performs remarkably well. At this height, the flow path has broadened significantly, as the upstream building is composed as a step-down notch with heights of 40 m and 23 m. Here, the flow is characterised by rather complex recirculating winds, which exhibit two peak directions corresponding to the SE–NW orientation of the canyon. The bimodal nature of the flow is very well reproduced in the LES. At the third comparison height ($z_{exp} = 45.5$ m) just above the roof-level of the upstream building, both flows have readjusted to the prescribed south-westerly inflow direction, resulting in comparable wind direction distributions.

Fig. 11 shows similar comparisons at different horizontal locations at the entrance into a courtyard (DM site; see Fig. 3). The entrance has a width of 14.5 m width. Horizontal spacings between the comparison locations are in the range of 6 m to 10 m. With heights of 32 m (upper building) and 30 m (lower building) the buildings forming the entrance are slightly lower compared to H . The wind roses are compared at two heights.

At the first comparison level, located at about half the local building height, LES and wind tunnel wind roses at the windward entrance (sites 01–04) are in very good agreement. Within the passage (sites 11–12), flow channelling resulted in higher velocity magnitudes and a narrowing of the frequency distributions compared to the impinging flow. The channelling effect is much stronger in the experiment, where the majority of observed instantaneous wind speeds are in the order of or larger than the reference velocity, U_{ref} , which corresponds to a much higher elevation. The strong width reduction of the LES wind roses goes hand in hand with a tendency towards decreased velocity variances in very narrow street canyons (Fig. 8).

At the second comparison layer, the agreement significantly increases at the windward and leeward passage exits. Within the passage, however, the LES wind roses clearly show a readjustment of the flow to the inflow direction. Here the widths of the distribution are comparable to those of the impinging, unobstructed flow (locations 01–04). This is not evident in the experiment, where the orientation of the wind roses still indicate topological flow channelling. These differences can be explained by the vertical offset of 0.5 m between numerical and experimental data pairs. That close to the local roof-level, where strong vertical velocity gradients have to be expected, such an offset can already have a significant influence on the comparability of the results.

5.2 Shape parameters

The above qualitative analysis of the shape and spread of experimental and LES frequency distributions is supported by a quantitative comparison of high-order statistical moments such as skewness (γ ; third moment), quantifying the symmetry of the distribution, and kurtosis (β ; fourth moment), measuring its peakedness [69]. For a normally distributed (Gaussian) data sample $\gamma = 0$ and $\beta = 3$. If $\gamma < 0$, the distribution is said to be left-skewed (longer left tail, centre of mass lies to the right). For $\gamma > 0$ the distribution is right-skewed (longer right tail). A leptokurtic distribution with $\beta > 3$ exhibits a higher peak and fatter tails than a Gaussian distribution, while the platykurtic counterpart ($\beta < 3$) is flat-topped with thin tails.

Fig. 12 shows height profiles of γ and β of the streamwise velocity component at four example locations. The parameters were derived from velocity samples for which such high-order statistics are meaningful, i.e. from unimodal distributions that further do not exhibit plateaus or extremely heavy tails. The scatter bars attached to the measurement data were derived from repetition measurements yielding a maximum range of ± 0.146 for γ and ± 0.203 for β . For the majority of points, the LES shape parameters fall well within the scatter of the

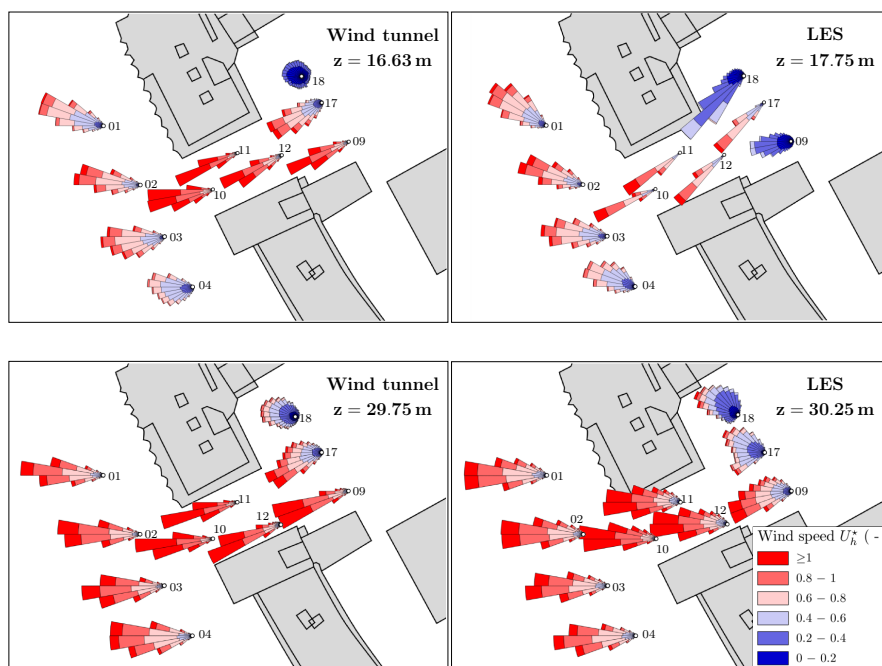


Fig. 11: Wind rose diagrams of wind tunnel (left) and LES (right) instantaneous horizontal wind speeds and directions at half the mean building height (approx. $0.5H$; top) and just below the mean building height (approx. $0.9H$; bottom) at the DM site. Note that the positions of the wind roses are not true to the exact (x,y) locations of the data points, but are shifted for a clearer display (see Fig. 3 for the exact locations). For the same reason, the percentage circles of the wind direction bars are omitted, but the same percentage range has been used in both cases. The map dimension is $90\text{ m} \times 70\text{ m}$. The flow is approaching from the left.

593 wind-tunnel equivalents. This statement holds for the rather unobstructed wind field above
 594 the Elbe river (BL04), but at comparison points further downstream within the inner city.
 595 The distinct vertical variability of skewness and kurtosis found at the intersection location
 596 BL10 is very well reproduced in the LES, which is an indication that the code is able to
 597 capture the flow structure at this site rather well.

598 Fig. 13 shows scatter plots of LES and wind tunnel high-order statistics derived from
 599 distributions of the instantaneous velocities U and V at the sub-sample of sites that where
 600 unimodal distributions were found. The majority of analysed LES and wind tunnel velocity
 601 signals exhibit more or less Gaussian shape characteristics. However, the scatter plots for
 602 γ reveal that there is a tendency towards a positive skewness of the U/U_{ref} signals (i.e. a
 603 trend toward tails at high velocities) in the experiment, while for the spanwise components,
 604 V/U_{ref} , more distributions are skewed to the left (tails at low velocities). These patterns are
 605 also seen in the LES. Offsets between the shape descriptors are more distinct for V/U_{ref} .
 606 More acute peaks and shorter tails ($\beta > 3$), for example, are observed in some of the LES ve-
 607 locity distributions. This trend of more leptokurtic LES velocities has been addressed in the

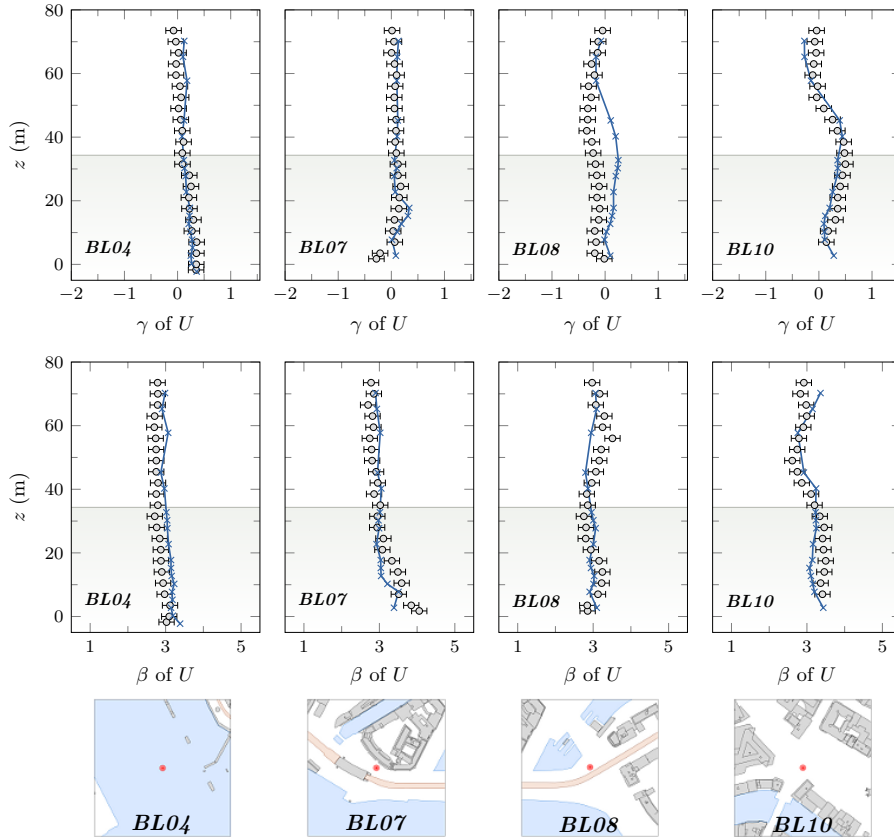


Fig. 12: Wind tunnel (dots) and LES (crosses) height profiles of skewness, γ (top), and kurtosis, β (bottom), of the streamwise velocity component at four sites. Heights below H are indicated by a grey shading.

608 previous section and is associated with physical and geometrical resolution characteristics
 609 in geometrically confined situations.

610 5.2.1 Wind direction fluctuations

611 In order to compare the time-dependency of statistical characteristics, we derive fluctuation
 612 time scales of the horizontal wind vector. Such an analysis is targeted at the quantification
 613 of typical time scales associated with a certain shift of the horizontal wind vector, which can
 614 be measured by direction differences as a function of time lag.

615 Results are presented for location BL04 above the Elbe river. Here the prevailing wind
 616 direction approximately agrees with the approach flow wind direction. Fluctuations of the
 617 horizontal wind direction are defined as $u'_d(t) = U_d(t) - \bar{U}_d$. Fig. 14 depicts frequency distributions
 618 of u'_d at four heights. The distributions reveal that the value range of the wind
 619 direction fluctuations is gradually narrowing with increasing distance from the ground as
 620 the distributions tend to become more peaked. Comparable height trends are present in both

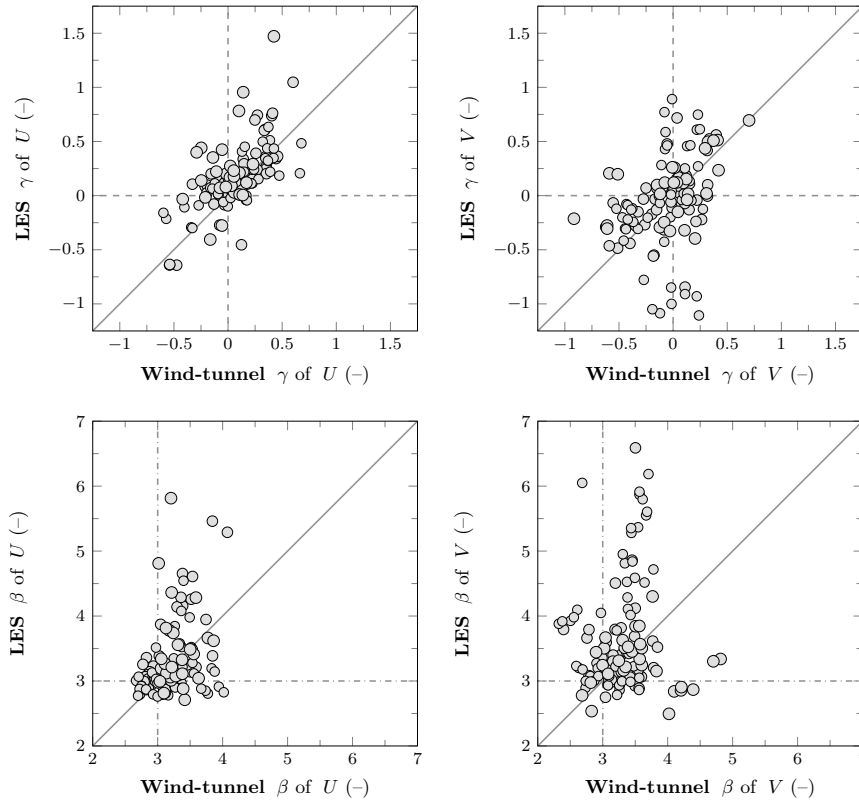


Fig. 13: Scatter plots of wind tunnel versus LES skewness, γ , and kurtosis, β , of the horizontal velocity components. Dashed lines indicate the Gaussian limits of $\gamma = 0$ and $\beta = 3$, while the solid line shows the 1:1 relationship.

621 data sets and there is a high level of agreement between spread and shape characteristics
 622 of experimental and LES distributions. This indicates that the latter is capturing the tran-
 623 sition between the stronger influence of smaller/short-lived eddies near the ground (high
 624 turbulence intensities) to larger/long-lived structures well above ground (low turbulence in-
 625 tensities).

626 Absolute differences of horizontal wind directions as a function of time lag, $|\delta U_d(t_l)|$,
 627 are compared in a next step (Fig. 15) as an indicator for the fluctuation intensity of the
 628 wind vector in the horizontal plane, which is essentially coupled to the structure of the flow.
 629 The evaluation is based on the median differences in order to account for the fact that the
 630 distributions tend to be strongly right-tailed. As a measure of observed value spread, the in-
 631 terquartile range (IQR) of the distributions (difference between the 75th and 25th percentile)
 632 is given as well. For this analysis, resampled (equally spaced) wind-tunnel time series were
 633 analysed (see Sect. 3.2.3). The time lag is defined as $t_l = n f^{-1}$, with $n = 0, \dots, N/2$ and N
 634 being the number of signals in the time series. The frequency, f , either refers to the sampling
 635 frequency of the LES, f_s , or to the mean data rate of the experiment, \dot{N} . Hence, while the
 636 time lags are the same at all heights in the LES since $f_s = \text{const}$, point-to-point differences
 637 are present for the experimental data because \dot{N} is location dependent. Fig. 15 shows results

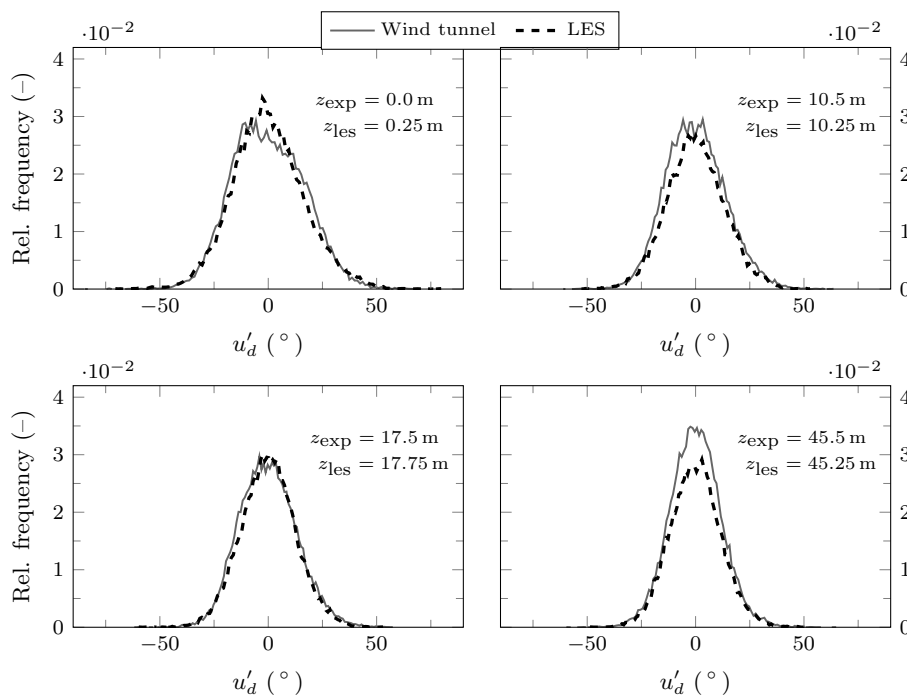


Fig. 14: Relative frequency distributions of horizontal wind direction fluctuations, u'_d , about the local time-average, \bar{U}_d , in the experiment (solid lines) and the LES (dashed lines) at four heights above the Elbe river (BL04). Note that the z -axis is defined with reference to ground level, to which the water level is vertically offset by -3.5 m.

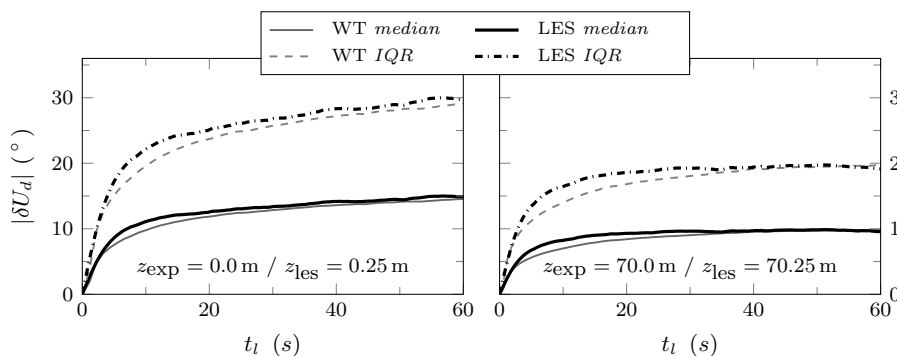


Fig. 15: Median absolute wind direction differences (wind tunnel: solid lines; LES: thick solid lines) together with the corresponding interquartile range (IQR; wind tunnel: dashed lines; LES: dash-dotted lines) as a function of full-scale time lag for a reference velocity of $U_{ref} = 5 \text{ m s}^{-1}$. The wind tunnel (WT) and LES data are displayed for two heights above the Elbe river (BL04).

638 for two heights above the river (BL04). The time lags are displayed in full-scale dimension,
639 using a reference wind speed of $U_{ref} = 5 \text{ m s}^{-1}$ for scaling. A high level of agreement be-
640 tween both data sets is found for the measures of central tendency and spread. The LES is
641 able to reproduce the experimental statistics on a point-by-point basis, but also with respect
642 to the overall time-development of the wind-angle differences as a function of height. At
643 both heights a relatively strong increase in the observed wind direction differences over the
644 first 10 s or so is followed by a pronounced flattening of the curves with a later levelling-off
645 into a plateau. The curves reveal a distinct height dependency, showing clearly as a decrease
646 with height of the median wind direction differences at the maximum displayed time lag of
647 $t_l = 60 \text{ s}$. This decrease is accompanied by a reduction of the spread of the underlying distri-
648 butions, in agreement with above results from the comparison of direction fluctuations. The
649 magnitude of the IQRs emphasise the variability in the angle-difference samples for a spec-
650 ified time lag. Even for small temporal offsets, the wind direction shifts can become quite
651 large due to the strong turbulent variability of the flow near the surface. This indicates how
652 low-frequency oscillations of the wind vector in the horizontal plane associated with larger-
653 scale eddies (longer time lags) are superimposed by high-frequency fluctuations, which are
654 stronger near the ground. The only systematic differences noticeable in the results shown in
655 Fig. 15 are seen in the slopes of the LES curves at small time lags, which are slightly higher
656 than their wind-tunnel counterparts, but then tend to level off faster.

657 6 Discussion and conclusions

658 This study aims to identify and test a strategy for an in-depth validation of eddy-resolving
659 simulations for turbulent flow in the near-surface atmospheric boundary layer. We propose
660 a three-level comparison procedure and test its applicability based on the example of urban
661 flow simulated with an implicit LES code. Detailed wind-tunnel measurements within a
662 realistic urban scale model provide the reference data.

663 6.1 Suitability of the reference experiment

664 It is necessary to confirm first that the reference experiment is suitable for a meaningful
665 and fair comparison with the simulation. The proposed validation strategy puts a strong
666 emphasis on the analysis of time series for the comparison of flow structures. Hence the
667 experimental data have to be of suitable quality for advanced signal processing and it has to
668 be verified that the laboratory measurements fulfil specific quality requirements. This con-
669 cerns the representativeness of the wind-tunnel model for the physical problem of interest
670 (similarity requirements), the qualification of the measured velocity data for advanced sig-
671 nal processing (signal quality and resolution properties), and the statistical robustness of
672 derived quantities (experimental reproducibility). For the test scenario covered in this study
673 the following was ensured:

- 674 – Geometric and dynamic similarity requirements are met by the experiment
- 675 – Inflow conditions comply with field observations and established standards for the phys-
676 ical modelling of turbulent boundary layers
- 677 – Signal durations are long enough to minimise the inherent uncertainty of derived statis-
678 tics and to perform a statistically representative analysis of large eddies in the flow (this
679 can be experimentally verified through temporal convergence tests of statistical quanti-
680 ties)

- 681 – Sampling frequencies are high enough to capture turbulence structures that are directly
- 682 resolved with LES
- 683 – The statistical reproducibility of experimental results, e.g. as derived from repetition
- 684 measurements, is documented
- 685 – The bias resulting from the resampling of LDA signals is quantifiable and minimised

686 Similar requirements regarding the quality and level of documentation of data and bound-
687 ary conditions of the experiment also apply to reference measurements carried out in the
688 field. Due to the natural variability of the atmosphere it is essential that the ambient me-
689 teorological conditions over the course of the field campaign are well documented at rep-
690 resentative locations in order to define the boundary conditions for the simulation [37]. In
691 complex environments like cities, it is also essential that sensor sites are characterised in
692 detail, e.g. regarding the local urban structure, surface cover or anthropogenic factors [48].

693 6.2 Exploratory data analysis

694 By applying the first level of the validation concept to the Hamburg test case we were able
695 to identify general features of the simulation in terms of mean flow and turbulence statistics
696 in comparison to the experiment at topologically different locations within the city. With
697 the analysis of frequency distributions the scene was set for a more in-depth comparison of
698 physical information hidden deeper within the time series.

699 *Mean flow characteristics* With this “traditional” comparison of mean flow and turbulence
700 statistics, typical obstacle-induced flow scenarios like recirculation zones, channelling ef-
701 fects or strong lateral flow deflections at street-level can be investigated. This type of anal-
702 ysis provides a valuable initial overview about how LES and experiment compare and is
703 helpful to identify cases of strong agreement or disagreement. The accuracy of the statistics
704 can be quantified by using sets of validation metrics, possibly in combination with estab-
705 lished quality acceptance thresholds. Discrepancies between LES and experiments should be
706 evaluated on a point-by-point basis. In this study, systematic quantitative differences were
707 determined, with the LES having a tendency to under-predict velocity magnitudes within the
708 UCL. This mostly affects locations where the flow path is strongly confined by surrounding
709 buildings. Depending on the alignment of the buildings within the numerical grid, some LES
710 sites are located closer to solid boundaries than in the wind tunnel as a result of the com-
711 paratively coarse obstacle representation through the blocking of entire grid cells. Another
712 factor affecting the comparability are spatial offsets between the wind tunnel and LES data
713 locations. Interpolating the LES data from the 2.5 m grid is not expected to mitigate this
714 issue in regions of strong velocity gradients. Here, spatial resolution properties of the exper-
715 imental data also have to be considered. For the test case, these are primarily determined by
716 the length of the LDA measuring volume (0.56 m full-scale). Such resolution and siting as-
717 pects need to be considered when dealing with highly three-dimensional, obstacle-induced
718 turbulence.

719 *Velocity sample characteristics* From the mean flow analysis alone no definite conclusions
720 about the agreement of the underlying data samples can or should be drawn; all informa-
721 tion available in the time series is condensed into single parameters. By exploring the value
722 range or occurrence probabilities of predicted quantities key reasons emerge to prefer time-
723 resolved methods over significantly less expensive steady-state RANS alternatives. A sim-
724 ple yet rarely pursued way to extend the exploratory assessment of a model’s predictive

725 skill is to focus on frequency distributions of velocities and derived quantities. Particularly
726 in cases where LES is not only intended to deliver reliable statistics, but also expected to
727 give an accurate account of the value range that can be expected (e.g. with regard to ex-
728 treme values) the comparison of frequency distributions is essential. The occurrence of bi-
729 modal and heavy-tailed velocity distributions is anything but rare in urban environments
730 and should be reproducible by eddy-resolving models. Comparisons of velocity and wind
731 direction histograms for the Hamburg test scenario showed that the LES captures complex
732 geometry-induced flow patterns realistically. In order to quantify this agreement, higher-
733 order distribution shape measures should be directly compared. For the case of unimodal
734 distributions, skewness and kurtosis parameters showed a very good agreement of associ-
735 ated height profiles at comparison points sufficiently far away from building façades. The
736 analysis of time scales and distributions of wind vector fluctuations in the horizontal plane
737 can provide additional information about the scales of eddies associated with shifts in wind
738 direction.

739 6.3 Outlook

740 With the concluding analysis of wind vector time scales, the study advanced towards an
741 important aspect of the LES validation problem: the comparison of time-related turbulence
742 statistics that are indicative of eddy structures in the flow. LES is expected to directly re-
743 solve the energy and flux-dominating turbulent eddies. Within urban areas, the size of the
744 largest eddies is restricted by the geometry and hence smaller than for example in the outer
745 regions of the surface layer. Hence it needs to be carefully evaluated whether the chosen
746 grid resolution (2.5 m in this case) is sufficient to represent UCL turbulence accurately. The
747 conclusions drawn about the agreement of mean flow and turbulence statistics should be
748 re-evaluated in light of the accuracy with which eddy scales are represented in the LES.
749 Comparing statistics associated with dominant scales of motion provides valuable insight
750 into the quality of the simulation. This is focused on in part II of the study by advancing the
751 “testing level” to the next stage by: (i) comparing turbulence features through an analysis of
752 integral time scales and energy density spectra; (ii) analysing the structure of the flow with
753 conditional resampling as part of the quadrant analysis of the vertical turbulent momentum
754 transfer and by using a wavelet transform method to compare the time-frequency content of
755 LES and laboratory flow.

756 **Acknowledgements** The numerical simulations with the LES code FAST3D-CT were carried out at the
757 Laboratories for Computational Physics and Fluid Dynamics of the U.S. Naval Research Laboratory in Wash-
758 ington D.C., USA. The authors wish to express their thanks to Jay Boris, Mi-Young Obenschain and other
759 collaborators there. Further thanks is given to colleagues at the Environmental Wind Tunnel Laboratory at the
760 University of Hamburg. Financial funding by the German Federal Office of Civil Protection and Disaster As-
761 sistance as well as by the Ministry of the Interior of the City of Hamburg within the “Hamburg Pilot Project” is
762 gratefully acknowledged (BBK research contract no. BBK III.1-413-10-364). Parts of the wind-tunnel model
763 construction were financially supported by the KlimaCampus at the University of Hamburg.

764 References

- 765 1. Guide for the Verification and Validation of Computational Fluid Dynamics Simulations (AIAA G-077-
766 1998(2002)). American Institute of Aeronautics and Astronautics, Inc. DOI doi:10.2514/4.472855.001
- 767 2. Adrian, R.J., Meneveau, C., Moser, R.D., Riley, J.: Final report on ‘Turbulence Measurements for LES’
768 workshop. Tech. rep., Department of Theoretical and Applied Mechanics, University of Illinois at
769 Urbana-Champaign, Urbana (IL), USA (2000)

- 770 3. Adrian, R.J., Yao, C.S.: Power spectra of fluid velocities measured by laser Doppler velocimetry. *Exp*
771 *Fluids* **5**, 17–28 (1987)
- 772 4. ASME: Guide for verification and validation in computational solid mechanics. ASME V&V 10-2006,
773 The American Society of Mechanical Engineers, New York (NY), USA (2006)
- 774 5. Book, D.L.: The conception, gestation, birth, and infancy of FCT. In: D. Kuzmin, R. Löhner, S. Turek
775 (eds.) *Flux-Corrected Transport: Principles, Algorithms, and Applications*, Scientific Computing, second
776 edn., pp. 1–21. Springer (2012)
- 777 6. Boris, J., Patnaik, G., Obenschain, K.: The how and why of Nomographs for CT-Analyst. Report
778 NRL/MR/6440-11-9326, Naval Research Laboratory, Washington (DC), USA (2011)
- 779 7. Boris, J.P.: New directions in computational fluid dynamics. *Annu Rev Fluid Mech* **21**, 345–385 (1989)
- 780 8. Boris, J.P.: On large eddy simulation using subgrid turbulence models. In: J.L. Lumley (ed.) *Whither*
781 *Turbulence? Turbulence at the Crossroads*, *Lecture Notes in Physics*, vol. 357, pp. 344–353. Springer
782 (1990)
- 783 9. Boris, J.P.: The threat of chemical and biological terrorism: Preparing a response. *Comput Sci Eng* **4**,
784 22–32 (2002)
- 785 10. Boris, J.P.: Dust in the wind: Challenges for urban aerodynamics. AIAA Paper 2005-5393 (2005)
- 786 11. Boris, J.P.: More for LES: A brief historical perspective of MILES. In: F.F. Grinstein, L.G. Margolin,
787 W.J. Rider (eds.) *Implicit Large Eddy Simulation: Computing Turbulent Fluid Dynamics*, pp. 9–38.
788 Cambridge University Press (2007)
- 789 12. Boris, J.P., Book, D.L.: Flux-corrected transport I: SHASTA – A fluid transport algorithm that works. *J*
790 *Comput Phys* **11**, 38–69 (1973)
- 791 13. Boris, J.P., Book, D.L.: Solution of the continuity equation by the method of flux-corrected transport. In:
792 B. Alder, S. Fernbach, M. Rotenberg, J. Killeen (eds.) *Methods in Computational Physics*, vol. 16, pp.
793 85–129. Academic Press (1976)
- 794 14. Bradshaw, P.: The understanding and prediction of turbulent flow. *Aeronaut J* **76**, 403–418 (1972)
- 795 15. Britter, R., Schatzmann, M. (eds.): Background and justification document to support the model evalua-
796 tion guidance and protocol. COST Action 732. University of Hamburg, Germany (2007a)
- 797 16. Britter, R., Schatzmann, M. (eds.): Model evaluation guidance and protocol document. COST Action
798 732. University of Hamburg, Germany (2007b)
- 799 17. Britter, R.E., Hanna, S.R.: Flow and dispersion in urban areas. *Annu Rev Fluid Mech* **35**, 469–496
800 (2003)
- 801 18. Chang, J.C., Hanna, S.R.: Air quality model performance evaluation. *Meteorol Atmos Phys* **87**, 167–196
802 (2004)
- 803 19. Cheng, W.C., Liu, C.H.: Large-eddy simulation of turbulent transports in urban street canyons in different
804 thermal stabilities. *J Wind Eng Ind Aerod* **99**, 434–442 (2011)
- 805 20. Counihan, J.: Adiabatic atmospheric boundary layers: A review and analysis of data from the period
806 1880 - 1972. *Atmos Environ* **9**, 871–905 (1975)
- 807 21. De Waele, S., Broersen, P.M.T.: Error measures for resampled irregular data. *IEEE T Instrum Meas* **49**,
808 216–222 (2000)
- 809 22. Edwards, R.V., Jensen, A.S.: Particle-sampling statistics in laser anemometers: sample-and-hold systems
810 and saturable systems. *J Fluid Mech* **133**, 397–411 (1983)
- 811 23. ESDU: Characteristics of atmospheric turbulence near the ground. Part II: single point data for strong
812 winds (neutral atmosphere). ESDU 85020, Engineering Sciences Data Unit, London, UK (1985)
- 813 24. Grimmond, C.S.B., Oke, T.R.: Aerodynamic properties of urban areas derived from analysis of surface
814 form. *J Appl Meteorol* **38**, 1262–1292 (1999)
- 815 25. Grinstein, F.F.: Verification and validation of CFD based turbulent flow experiments. In: *Encyclopedia*
816 *of Aerospace Engineering*, pp. 515–523. John Wiley & Sons (2010)
- 817 26. Hanna, S., Chang, J.: Acceptance criteria for urban dispersion model evaluation. *Meteorol Atmos Phys*
818 **116**(3), 133–146 (2012)
- 819 27. Hanna, S.R., Brown, M.J., Camelli, F.E., Chan, S.T., Coirier, W.J., Kim, S., Hansen, O.R., Huber, A.H.,
820 Reynolds, R.M.: Detailed simulations of atmospheric flow and dispersion in downtown manhattan: An
821 application of five computational fluid dynamics models. *B Am Meteorol Soc* **87**(12), 1713–1726 (2006)
- 822 28. Hanna, S.R., Hansen, O.R., Dharmavaram, S.: FLACS CFD air quality model performance evaluation
823 with Kit Fox, MUST, Prairie Grass, and EMU observations. *Atmos Environ* **38**, 4675–4687 (2004)
- 824 29. Hertwig, D.: On Aspects of Large-Eddy Simulation Validation for Near-Surface Atmo-
825 spheric Flows. Ph.D. thesis, Universität Hamburg (2013). URL [http://ediss.sub.uni-](http://ediss.sub.uni-hamburg.de/volltexte/2013/6289/pdf/Dissertation.pdf)
826 [hamburg.de/volltexte/2013/6289/pdf/Dissertation.pdf](http://ediss.sub.uni-hamburg.de/volltexte/2013/6289/pdf/Dissertation.pdf)
- 827 30. Hertwig, D., Efthimiou, G.C., Bartzis, J.G., Leitl, B.: CFD-RANS model validation of turbulent flow in
828 a semi-idealized urban canopy. *J Wind Eng Ind Aerod* **111**, 61–72 (2012)
- 829 31. Hertwig, D., Leitl, B., Schatzmann, M.: Organized turbulent structures – Link between experimental data
830 and LES. *J Wind Eng Ind Aerod* **99**, 296–307 (2011)

- 831 32. Huang, H., Ooka, R., Kato, S.: Urban thermal environment measurements and numerical simulation for
832 an actual complex urban area covering a large district heating and cooling system in summer. *Atmos*
833 *Environ* **39**(34), 6362–6375 (2005)
- 834 33. Kaimal, J.C., Wyngaard, J.C., Izumi, Y., Coté, O.R.: Spectral characteristics of surface-layer turbulence.
835 *Q J Roy Meteor Soc* **98**, 563–589 (1972)
- 836 34. Kanda, M.: Progress in urban meteorology: A review. *J Meteorol Soc Jpn Ser. II* **85B**, 363–383 (2007)
- 837 35. Kempf, A.M.: LES validation from experiments. *Flow Turbul Combust* **80**, 351–373 (2008)
- 838 36. Konow, H.: Tall Wind Profiles in Heterogeneous Terrain. Ph.D. thesis, Universität Hamburg (2015).
839 URL <http://ediss.sub.uni-hamburg.de/volltexte/2015/7202/pdf/Dissertation.pdf>
- 840 37. Leitl, B.: Validation data for microscale dispersion modelling. *EUROTRAC Newsletter* **22**, 28–32 (2000)
- 841 38. Li, X.X., Britter, R.E., Koh, T.Y., Norford, L.K., Liu, C.H., Entekhabi, D., Leung, D.Y.C.: Large-eddy
842 simulation of flow and pollutant transport in urban street canyons with ground heating. *Bound-Lay*
843 *Meteorol* **137**, 187–204 (2010)
- 844 39. Li, X.X., Britter, R.E., Norford, L.K., Koh, T.Y., Entekhabi, D.: Flow and pollutant transport in urban
845 street canyons of different aspect ratios with ground heating: Large-eddy simulation. *Bound-Lay Mete-*
846 *orol* **142**, 289–304 (2012)
- 847 40. Li, X.X., Liu, C.H., Leung, D.Y.C., Lam, K.M.: Recent progress in CFD modelling of wind field and
848 pollutant transport in street canyons. *Atmos Environ* **40**, 5640–5658 (2006)
- 849 41. Liu, Y.S., Cui, G.X., Wang, Z.S., Zhang, Z.S.: Large eddy simulation of wind field and pollutant disper-
850 sion in downtown Macao. *Atmos Environ* **45**, 2849–2859 (2011)
- 851 42. Mochida, A., Lun, I.: Prediction of wind environment and thermal comfort at pedestrian level in urban
852 area. *J Wind Eng Ind Aerod* **96**, 1498–1527 (2008)
- 853 43. Moonen, P., Defraeye, T., Dorer, V., Blocken, B., Carmeliet, J.: Urban physics: Effect of the micro-
854 climate on comfort, health and energy demand. *Front Archit Res* **1**, 197–228 (2012)
- 855 44. Moonen, P., Gromke, C., Dorer, V.: Performance assessment of large eddy simulation (LES) for modeling
856 dispersion in an urban street canyon with tree planting. *Atmos Environ* **75**, 66–76 (2013)
- 857 45. Murakami, S., Ooka, R., Mochida, A., Yoshida, S., Kim, S.: CFD analysis of wind climate from human
858 scale to urban scale. *J Wind Eng Ind Aerod* **81**, 57–81 (1999)
- 859 46. Oberkampf, W.L., Barone, M.F.: Measures of agreement between computation and experiment: Validation
860 metrics. *J Comput Phys* **217**, 5–36 (2006)
- 861 47. Oberkampf, W.L., Trucano, T.G.: Verification and validation in computational fluid dynamics. *Prog*
862 *Aerosp Sci* **38**, 209–272 (2002)
- 863 48. Oke, T.R.: Siting and exposure of meteorological instruments at urban sites. In: C. Borrego, A.L. Norman
864 (eds.) *Air Pollution Modeling and its Application XVII*, chap. 66, pp. 615–631. Springer (2007)
- 865 49. Park, S.B., Baik, J.J., Raasch, S., Letzel, M.O.: A large-eddy simulation study of thermal effects on
866 turbulent flow and dispersion in and above a street canyon. *J Appl Meteorol Climatol* **51**, 829–841
867 (2012)
- 868 50. Patnaik, G., Boris, J.P., Grinstein, F.F., Iselin, J.P., Hertwig, D.: Large scale urban simulations with
869 FCT. In: D. Kuzmin, R. Löhner, S. Turek (eds.) *Flux-Corrected Transport: Principles, Algorithms, and*
870 *Applications*, Scientific Computing, second edn., pp. 91–117. Springer (2012)
- 871 51. Patnaik, G., Grinstein, F.F., Boris, J.P., Young, T.R., Parmhed, O.: Large-scale urban simulations. In: F.F.
872 Grinstein, L.G. Margolin, W.J. Rider (eds.) *Implicit Large Eddy Simulation: Computing Turbulent Fluid*
873 *Dynamics*. Cambridge University Press (2007)
- 874 52. Plate, E.J.: Methods of investigating urban wind fields – physical models. *Atmos Environ* **33**, 3981–3989
875 (1999)
- 876 53. Ramond, A., Millan, P.: Measurements and treatment of LDA signals, comparison with hot-wire signals.
877 *Exp Fluids* **28**, 58–63 (2000)
- 878 54. Salim, S.M., Buccolieri, R., Chan, A., Di Sabatino, S.: Numerical simulation of atmospheric pollutant
879 dispersion in an urban street canyon: Comparison between RANS and LES. *J Wind Eng Ind Aerod* **99**,
880 103–113 (2011)
- 881 55. Schatzmann, M., Leitl, B.: Validation of urban flow and dispersion CFD models. In: *Proceedings of the*
882 *5th International Symposium on Computational Wind Engineering*. Chapel Hill, North Carolina (2010)
- 883 56. Schatzmann, M., Olesen, H., Franke, J. (eds.): *COST 732 model evaluation case studies: Approaches*
884 *and results*. COST Action 732. University of Hamburg, Germany (2010). ISBN 3-00-018312-4
- 885 57. Schlünzen, K.H.: On the validation of high-resolution atmospheric mesoscale models. *J Wind Eng Ind*
886 *Aerod* **67/68**, 479–492 (1997)
- 887 58. Simiu, E., Scanlan, R.H.: *Wind Effects on Structures*, 2nd edn. John Wiley & Sons, New Jersey (1986)
- 888 59. Standen, N.M.: A spire array for generating thick turbulent shear layers for natural wind simulation in
889 wind tunnels. Report LTR-LA-94, National Aeronautical Establishment, Canada (1972)
- 890 60. Stathopoulos, T.: Pedestrian level winds and outdoor human comfort. *J Wind Eng Ind Aerod* **94**, 769–780
891 (2006)

- 892 61. Tamura, T.: Towards practical use of LES in wind engineering. *J Wind Eng Ind Aerod* **96**, 1451–1471
893 (2008)
- 894 62. Tominaga, Y., Mochida, A., Yoshie, R., Kataoka, H., Nozu, T., Yoshikawa, M., Shirasawa, T.: AIJ guide-
895 lines for practical applications of CFD to pedestrian wind environment around buildings. *J Wind Eng*
896 *Ind Aerod* **96**, 1749–1761 (2008)
- 897 63. Tominaga, Y., Stathopoulos, T.: CFD modeling of pollution dispersion in a street canyon: Comparison
898 between LES and RANS. *J Wind Eng Ind Aerod* **99**, 340–348 (2011)
- 899 64. Tominaga, Y., Stathopoulos, T.: CFD modeling of pollution dispersion in building array: Evaluation of
900 turbulent scalar flux modeling in RANS model using LES results. *J Wind Eng Ind Aerod* **104-106**,
901 484–491 (2012)
- 902 65. Tominaga, Y., Stathopoulos, T.: CFD simulation of near-field pollutant dispersion in the urban environ-
903 ment: A review of current modeling techniques. *Atmos Environ* **79**, 716–730 (2013)
- 904 66. VDI: Environmental meteorology – Physical modelling of flow and dispersion processes in the atmo-
905 spheric boundary layer – Application of wind tunnels. Guideline VDI-3783-12, Verein Deutscher Inge-
906 nieure (The Association of German Engineers), Beuth Verlag, Berlin (2000)
- 907 67. VDI: Environmental meteorology – Prognostic microscale wind field models – Evaluation for flow
908 around buildings and obstacles. Guideline VDI-3783-9, Verein Deutscher Ingenieure (The Association
909 of German Engineers), Beuth Verlag, Berlin (2005)
- 910 68. Wettermast Hamburg, Universität Hamburg: URL <http://www.wettermast-hamburg.zmaw.de>
- 911 69. Wilks, D.S.: Statistical Methods in the Atmospheric Sciences, 2nd edn. Academic Press, Waltham (MA)
912 (2005)
- 913 70. Winter, A.R., Graham, L.J.W., Bremhorst, K.: Effects of time scales on velocity bias in LDA measure-
914 ments using sample and hold processing. *Exp Fluids* **11**, 147–152 (1991)
- 915 71. Wyngaard, J.C., Peltier, L.J.: Experimental micrometeorology in an era of turbulence simulation. *Bound-*
916 *Lay Meteorol* **78**, 71–86 (1996)
- 917 72. Xie, Z.T., Castro, I.P.: LES and RANS for turbulent flow over arrays of wall-mounted obstacles. *Flow*
918 *Turbul Combust* **76**, 291–312 (2006)
- 919 73. Xie, Z.T., Castro, I.P.: Large-eddy simulation for flow and dispersion in urban streets. *Atmos Environ*
920 **43**, 2174–2185 (2009)
- 921 74. Xie, Z.T., Hayden, P., Wood, C.: Large-eddy simulation of approaching-flow stratification on dispersion
922 over arrays of buildings. *Atmos Environ* **71**, 64–74 (2013)